# HIGHWAY RESEARCH RECORD

## Number 30

# Culverts and Slope Protection

4 Reports

Presented at the
42nd ANNUAL MEETING
January 7-11, 1963

HIGHWAY RESEARCH BOARD
of the
Division of Engineering and Industrial Research
National Academy of Sciences—
National Research Council
Washington, D. C.
1963

## *Department of Materials and Construction*

John H. Swanberg, Chairman
Minnesota Department of Highways
St. Paul

GENERAL MATERIALS DIVISION

C. E. Minor, Chairman
Materials and Research Engineer
Washington Department of Highways, Olympia

M. G. Spangler, Vice Chairman
Iowa State University, Ames

COMMITTEE ON CULVERTS AND CULVERT PIPE

M. G. Spangler, Chairman
Iowa State University, Ames

John L. Beaton, Materials & Research Engineer, California Division of Highways, Sacramento
T. F. DeCapiteau, Drainage Products Engineer, Manufacturing Division, Republic Steel Corporation, Youngstown, Ohio
W. B. Drake, Assistant State Highway Engineer, Kentucky Department of Highways, Lexington
Kenneth S. Eff, Chief, Hydraulic Section, Civil Engineering Branch, Office, Chief of Engineers, Department of the Army, Washington, D. C.
Ralph Fadum, Head, Civil Engineering Department, State College of Agriculture & Engineering of the University of North Carolina, Raleigh
C. J. Francis, Director, Engineering Division, Soil Conservation Service, U. S. Department of Agriculture, Washington, D. C.
R. T. Healy, Executive Secretary, Connecticut Concrete Pipe Association, Inc., South Windham
John G. Hendrickson, Jr., Director of Engineering Research, American Concrete Pipe Association, Chicago, Illinois
A. H. Koepf, Manager, Field Engineering—Highway Products, Kaiser Aluminum and Chemical Sales, Inc., Oakland, California
J. Alan Myers, United States Steel Corporation, Pittsburgh, Pennsylvania
C. E. Proudley, Director of Engineering & Executive Secretary, The Carolinas Ready Mix Concrete Association, Inc., Raleigh, N. C.
E. P. Sellner, Manager, Conservation Bureau, Portland Cement Association, Chicago, Illinois
Rockwell Smith, Research Engineer—Roadway, Association of American Railroads, Chicago, Illinois
Reynold K. Watkins, Head, Mechanical Engineering Department, Utah State University, Logan
H. L. White, Chief Sales Engineer, Armco Drainage & Metal Products, Inc., Middletown, Ohio

## *Department of Design*

T. E. Shelburne, Chairman
Director of Research, Virginia Department of Highways
Charlottesville

### COMMITTEE ON SURFACE DRAINAGE OF HIGHWAYS

Carl F. Izzard, Chairman
Chief, Hydraulic Research Division, Office of Research and Development
U. S. Bureau of Public Roads, Washington, D.C.

Robert E. Bond, Hydraulic Engineer, Region 9, U. S. Bureau of Public Roads, Denver, Colorado
Tate Dalrymple, U. S. Geological Survey, Washington, D. C.
Roy C. Edgerton, Assistant Engineer of Design, Highway Research Board, Washington, D. C.
Kenneth S. Eff, Chief, Hydraulic Section, Office, Chief of Engineers, Department of the Army, Washington, D. C.
John G. Hendrickson, Jr., Director of Engineering Research, American Concrete Pipe Association, Chicago, Illinois
S. W. Jens, Consulting Engineer, St. Louis, Missouri
Frank L. Johnson, Hydraulic Engineer, Region 6, U. S. Bureau of Public Roads, Fort Worth, Texas
Clint Jay Keifer, Engineer of Sewer Hydraulics, City Bureau of Engineering, Chicago, Illinois
A. H. Koepf, Manager, Field Engineering—Highway Products, Kaiser Aluminum & Chemical Sales, Inc., Oakland, California
Robert A. Norton, Bridge Engineer, Connecticut State Highway Department, Wethersfield
Ralph M. Peterson, Assistant Chief, Civil Engineering Branch, Division of Engineering, U. S. Department of Agriculture, Washington, D. C.
A. L. Pond, Jr., Hydraulic Engineer, Virginia Department of Highways, Richmond
W. O. Ree, Agricultural Research Service, Stillwater, Oklahoma
John M. Robertson, Manager, Drainage & Allied Products Sales, Armco Steel Corporation, Middletown, Ohio
Edwin R. Rowe, California Division of Highways, San Francisco, California
James K. Searcy, Hydraulic Engineer, Hydraulic & Hydrological Branch, U. S. Bureau of Public Roads, Washington, D. C.
F. W. Thorstenson, Preliminary Design Engineer, Minnesota Department of Highways, St. Paul
W. S. Winslow, Assistant Chief Engineer—Bridges, North Carolina State Highway Commission, Raleigh

# Contents

# Strength of Steel Culvert Sheets Bearing Against Compacted Sand Backfill

G. G. MEYERHOF, Director, School of Graduate Studies, Nova Scotia Technical College, Halifax, and
L. D. BAIKIE, Engineer, Materials Testing Laboratory, Department of Public Works, Ottawa, Ontario

As part of a study of the strength of corrugated metal culverts under fills, an investigation has been made of the ultimate load of curved steel sheets bearing against dense sand backfill. The loading tests were carried out at a scale of one-eight full size by applying an axial load at the end of plain and corrugated sheets of various thicknesses and radii of curvature. During the tests measurements were made of the strains, soil pressures and deflections of the sheets.

The stress-deformation and strength characteristics of the sand were determined by triaxial compression tests from which representative values of the coefficient of soil reaction ("subgrade modulus") were calculated. These values were found to be of the same order as the average coefficients deduced from the loading tests on the sheets. Using these coefficients, the theoretical ultimate load of the sheets was determined from an analysis based on an extension of the theory of elastic stability of plates to the problem of curved sheets supported by an elastic medium.

The analysis shows that for small values of the coefficient of soil reaction or modulus of deformation of the soil, and for small values of the flexural rigidity of the plates, the sheets would fail by buckling, but for larger values of these parameters the sheets would fail by yielding of the section. The observed ultimate loads and modes of failure of the sheets were in reasonable agreement with these estimates and also support the ring compression theory.

An analysis is also made of the strength of flexible culverts under fills, for which simple equations and design charts are presented. From the results of field observations on the deformation of flexible culverts, minimum values of the coefficient of soil reaction and modulus of deformation of fills are suggested to insure that the critical stresses are sensibly independent of the culvert diameter. The results of some earlier model tests on the buckling of flexible culverts support the proposed method of analysis, which can be used in conjunction with the ring compression theory to estimate the strength of culverts under fills in practice.

• THE RAPID expansion of modern transportation facilities requires the construction of numerous culverts and other underground structures. Since many of these installations are of greater size and subjected to larger loads than those built previously,

---

Paper sponsored by Committee on Culverts and Culvert Pipe.

an estimate of the strength of such structures has to be based on an extension of previous experience through rational methods of design.

One of the best known analyses of the behavior of flexible circular culverts under an earth fill is that of Spangler (3) who extended Marston's theory of loads on underground pipes. In this method the vertical pressures are assumed to be uniformly distributed over the pipe diameter at the top and over the bedding width at the bottom of the culvert. The horizontal pressure is assumed to be distributed parabolically over the middle $100^0$ arc of the pipe, and the resulting stresses and deflection of the pipe are evaluated. This approach has recently been simplified by White (8) who assumed a uniform pressure distribution around flexible pipes with sufficient cover and good backfill so that the strength of culverts can then be estimated from the simple theory of ring compression.

Both methods neglect instability of culverts due to buckling which was discussed by Watkins (6) on the assumption of a uniform pressure distribution around circular culverts. Since buckling may govern the strength of larger culverts and the pressure distribution around such structures is not necessarily uniform, an investigation was made at the Nova Scotia Technical College of the ultimate load of steel culvert sheets bearing against dense sand backfill. The loading tests were carried out at a scale of one-eighth full size, and measurements were made of the strains, soil pressures and deflections of the sheets (1). This report summarizes the main test results and extends previous analyses to an estimate of the ultimate strength of flexible culverts in practice.

## METHOD AND RESULTS OF MODEL TESTS

Underground flexible culverts frequently have their critical sections in the lower quadrants due to difficulties of obtaining a uniform backfill. Quarter-sections of a circular culvert were therefore selected for the present tests, and for testing convenience and analysis, an axial load was applied directly to the end of the sheets (Fig. 1). This loading condition is more severe than that found in practice where the load is applied to culverts through an earth fill.

The model tests were carried out in a steel box about $4\frac{1}{2}$ ft long, 2 ft wide and 3 ft high (Fig. 1). The plain and corrugated steel sheets had about a 19-in. width and 12- and 24-in. nominal radii. The physical properties of the steel culvert sheets are given in Table 1. Electric resistance strain gages, soil pressure gages and dial deflectometers were mounted along the central arc of the sheets (Fig. 1). The soil pressure gages consisted of lead plates of $\frac{1}{2}$-in. diameter and $\frac{1}{16}$-in. thickness, which were indented by $\frac{1}{8}$-in. diameter steel balls attached to the sheets. Using a calibration curve based on the average duration of the tests, the maximum soil pressures could readily be deduced from the diameter of the indentation in the lead.

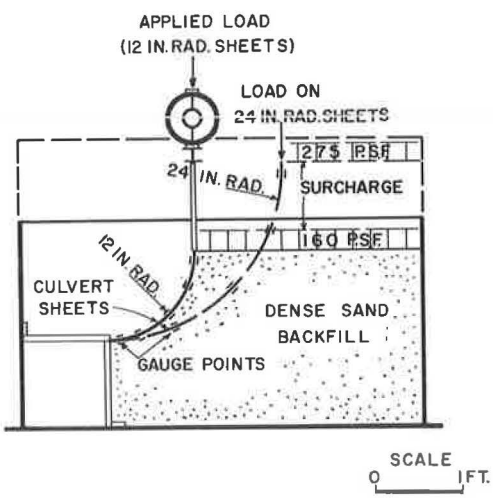


Figure 1. General arrangement of loading tests.

During the backfilling and compaction of the dry sand (Table 2), the sheets were supported by bracing. This was removed before a surcharge was placed on the sand, representing the weight of the soil above the centerline of the culvert plus a 3-ft cover at $\frac{1}{8}$ scale of the tests. The upper and lower edges of the sheets were free to rotate during the tests, and in some cases an attempt was made to prevent shear at the upper edge by allowing horizontal movement of the load.

The main test results are summarized in Table 3. It was found that both stresses and radial deflections of the sheets increased roughly linearly with the load until

TABLE 1

PROPERTIES OF STEEL CULVERT SHEETS

| Sheet Type | Test No. | Radius, r (in.) | Thickness, t (in.) | Area, A ( sq in.) | Yield Stress, $f_y$ (psi) |
|---|---|---|---|---|---|
| Plain | 1 and 2 | 12 | 0.042 | 0.788 | 45,000 |
| | 3 and 4 | 12.9 | 0.042 | 0.788 | 45,000 |
| | 5[a] | 12.9 | 0.017 | 0.319 | 35,000 |
| | 6 | 25.6 | 0.042 | 0.788 | 45,000 |
| | 7[a], 8[a], and 9 | 12.9 | 0.017 | 0.319 | 35,000 |
| Corrugated[b] | 10 | 12 | 0.017 | 0.427 | 30,000 |
| | 11 | 24 | 0.017 | 0.386 | 30,000 |
| | 12 | 24 | 0.017 | 0.388 | 30,000 |
| | 13 | 12 | 0.017 | 0.396 | 30,000 |

[a]No shear test.
[b]Corrugations: 1/4 x 3/4 in.

TABLE 2

PROPERTIES OF SAND BACKFILL[a]

| | |
|---|---|
| Effective size, $d_{10}$ | 0.16 mm |
| Uniformity coeff., U | 5.0 |
| Avg. unit weight, w | 116 pcf |
| Relative density, $D_r$ | 0.9 |
| Angle of intnl. frict., $\phi$ | $40^0$ |

[a]Grading limits: No. 200 to 4 U.S.S.sieve.

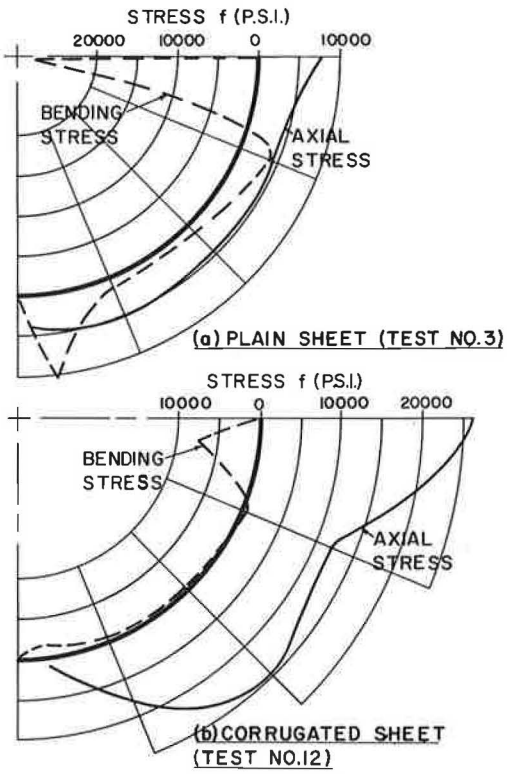


Figure 2. Stresses in sheets at ultimate load.

failure was reached, except near the critical section where the increase was more rapid as the ultimate load was approached. At any given load, the observed axial stresses decreased with distance from the upper edge of the sheet (Fig. 2) on account of the skin friction between the sheets and the sand, and the deduced angle of skin friction of about $20^0$ agrees well with previous investigations for smooth metal (2). Because of this skin friction and the limited lateral restraint near ground level, failure of the sheets occurred within the upper 2 in. in most tests. The average radial failure strain was generally of the order of 1/4 to 1/2 percent of the radius of the sheets; the corresponding vertical strain at the upper edge was about 1/2 to 1 percent of the radius of the sheets.

All plain sheets failed by buckling and, omitting the exceptionally low value of test No. 1 due to accidental eccentricity of the load, the average failure stress of the thin sheets was about 7,100 psi and for thick sheets about 5,600 psi. Both values represent about 16 percent of the corresponding yield stress of the material. The sheets without

TABLE 3

RESULTS OF LOADING TESTS ON CULVERT SHEETS

| Test No. | Obs. Ult. Load, $P_o$ (lb) | Max. Axial Stress, $f_o$ (psi) | Avg. Soil Pressure, p (psi) | Avg. Radial Deflect., d (in.) | Avg. Coef. of Soil React., k (pci) | Theoret. Ring Stress, Eq. 1, $f_a$ (psi) | Theoret. Critical Stress, Eq. 2, $f_c$ (psi) |
|---|---|---|---|---|---|---|---|
| 1 | 1,730[a] | 2,190[a] | 5.0 | 0.013 | 385 | 1,540 | 12,000 |
| 2 | 5,000 | 6,350 | 8.6 | 0.043 | 200 | 2,640 | 8,820 |
| 3 | 6,180 | 7,850 | 3.6 | 0.076 | 45 | 1,100 | 4,200 |
| 4 | 6,900 | 8,770 | 11.9 | 0.074 | 160 | 3,680 | 7,800 |
| 5 | 1,840 | 5,780 | 8.1 | 0.022 | 370 | 6,160 | 6,920 |
| 6 | 4,400 | 5,600 | 5.9 | 0.057 | 105 | 3,380 | 6,250 |
| 7 | 2,490 | 7,800 | 8.3 | 0.029 | 285 | 6,290 | 6,000 |
| 8 | 1,500 | 4,690 | 6.9 | 0.026 | 260 | 5,250 | 5,780 |
| 9 | 1,270 | 3,980 | 7.0 | 0.015 | 465 | 5,290 | 7,750 |
| 10 | 14,200 | 33,300 | 48.1 | 0.224 | 215 | 33,900 | (97,000) |
| 11 | 7,800 | 20,100 | 6.6 | 0.029 | 225 | 9,310 | (100,000) |
| 12 | 10,100 | 26,100 | 3.7 | 0.030 | 125 | 5,230 | (73,000) |
| 13 | 16,400 | 41,400 | 36.7 | 0.432 | 85 | 25,900 | (60,000) |

[a]Low value due to eccentric load.

shear at the upper edge carried somewhat larger loads than those with shear as would be expected. On the other hand, the corrugated sheets generally failed by crushing at an average stress of about 30,000 psi which is the same as the yield stress of the steel. Except near the critical section and lower edge, the bending stresses in the sheets were small and amounted to about $\frac{1}{4}$ to $\frac{1}{2}$ the axial stresses at failure in the central portion of the sheets (Fig. 2).

Although the distribution of the soil pressure on the sheets at failure is similar to the maximum radial deflections, the observed coefficients of soil reaction (ratios of soil pressure to radial deflection) varied considerably around the sheets and increased as the radial deflection decreased (Fig. 3). Therefore, the average values of the soil pressure, radial deflection and coefficient of soil reaction (Table 3) were obtained by dividing the total volume under the pressure and deflection curves by the area of the sheets in contact with the sand.

## ANALYSIS OF TEST RESULTS

If the flexural rigidity of the sheets is ignored, the average axial stress $f_a$ in a cylindrical plate can be estimated from the theory of ring compression (8) so that

$$f_a = p\,r/A \qquad (1)$$

in which

p = average soil pressure on plate;
r = radius of plate; and
A = cross-sectional area of plate.

Using the average observed soil pressures at failure and the original radius of the sheets, the calculated ring stresses are found to be of a similar order of magnitude as the observed maximum axial stresses (Table 3). The main differences between the estimates and observations are associated with low soil pressures for which the pressure gages were rather insensitive.

Another estimate of the failure stresses can be obtained from the theory of elastic stability of plates (5). If a cylindrical plate bearing against compact soil is compressed by a uniformly distributed force acting on the straight and hinged edges, the theoretical buckling stress is

$$f_b = \frac{2}{A}\sqrt{\frac{kEI}{1-m^2}} \qquad (2)$$

in which

A = cross-sectional area of plate;
E = modulus of elasticity of plate;
I = moment of inertia of plate;
k = coefficient of soil reaction (subgrade modulus); and
m = Poisson's ratio of plate.

The maximum value of the buckling stress $f_b$ is given by the yield stress $f_y$ of the plate (see Appendix).

The average values of the coefficient of soil reaction k can be approximately determined from the modulus of deformation $E_s$ of the soil in triaxial compression tests under a lateral pressure equal to the average confinement pressure of the soil (4), which was about 10 psi at the center of the sheets at failure. Making an 18-in. allowance behind the sheets for the limited width of backfill, the coefficients of soil reaction deduced from triaxial compression tests on the sand are shown in Figure 4 together with the average values obtained from the loading tests. While these coefficients are roughly inversely proportional to the radial deflection, the coefficients from the loading tests are somewhat larger than the values deduced from the triaxial compression tests because of the skin friction between the sand and both the sheets and the steel box. This makes the sand appear to be stiffer than assumed.

Using the coefficients of soil reaction from the loading tests, the critical stresses estimated from Eq. 2 are given in Table 3. The estimated critical stresses compare reasonably well with the observed maximum values and also support the observed mode of failure of the sheets. Thus, the estimates show that the plain sheets are expected to fail by buckling at a stress of the order of one-sixth of the yield stress of the steel, while the corrugated sheets are expected to fail by crushing at the

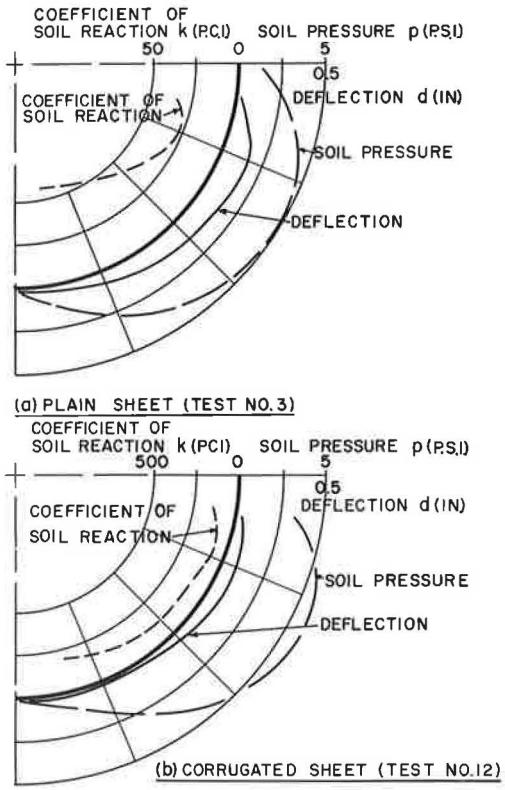


Figure 3. Soil pressures, deflections, and coefficients of soil reaction for sheets at ultimate load.

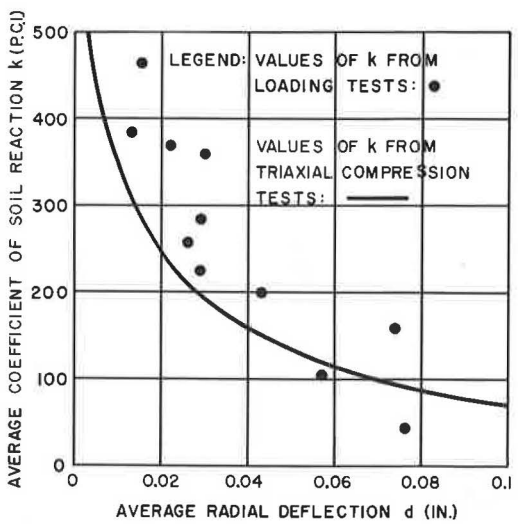


Figure 4. Coefficients of soil reaction from loading tests and triaxial compression tests.

yield stress since their theoretical buckling stress is some 2 to 4 times the yield stress.

## STRENGTH OF FLEXIBLE CULVERTS

Experience with underground flexible culverts has shown (8) that their flexural rigidity governs mainly the installation stages, while the compressive strength of the culvert material or joints governs the behavior under load as in a thin compression ring provided there is adequate backfill. The corresponding ring compression theory (Eq. 1) has been used successfully to design thin-walled plain and corrugated metal structures of different shapes, sizes and depths of backfill compacted to about 95 percent of the standard Proctor density. However, this approach does not take into account the actual properties of soils which may vary within wide limits, even at a specified Proctor density. Moreover, buckling may become important for larger structures than those built to date.

Therefore, in conjunction with the present model tests, a method has been developed to estimate the critical buckling stress of underground flexible culverts. As shown in the Appendix, the critical stress $f_c$ of a circular culvert can be represented by

$$f_c = \frac{f_y}{1 + \frac{f_y (1 - m^2) A r^2}{C E I}} \tag{3}$$

in which

$A$ = effective cross-sectional area of culvert material;
$C$ = buckling coefficient;
$E$ = effective modulus of elasticity of culvert material;
$f_y$ = effective yield stress of culvert material;
$I$ = effective moment of inertia of culvert material;
$m$ = Poisson's ratio of culvert material; and
$r$ = radius of culvert.

For fills of which the deformation properties can be represented by a coefficient of soil reaction k, the theoretical buckling coefficients $C_k$ have been derived in the Appendix. These coefficients are shown in Figure 5 in terms of the ratio $r/L_k$, where $L_k$ is the relative stiffness of the culvert with respect to the soil and is

$$L_k = \sqrt[4]{\frac{E I}{(1 - m^2) k}} \tag{4}$$

Further, it is shown for the important practical case of $r/L_k > 2$ that Eq. 3 can be simplified to

$$f_c = \frac{f_y}{1 + \frac{f_y A}{2} \sqrt{\frac{1 - m^2}{k E I}}} \tag{5}$$

which is analogous to Eq. 2 and makes some allowance for accidental eccentricities and imperfections which can be expected in practice.

Frequently the deformation properties of fills are more closely represented by a modulus of deformation $E_s$ and Poisson's ratio $m_s$. The corresponding theoretical buckling coefficients $C_e$ have also been derived in the Appendix and are shown in Figure 5 in terms of the ratio $r/L_e$, where the relative stiffness

$$L_e = \sqrt[3]{\frac{2\,(1 - m_s^2)\,EI}{(1 - m^2)\,E_s}} \qquad (6)$$

Further, Eq. 3 yields for $r/L_e > 2$

$$f_c = \frac{f_y}{1 + f_y A \sqrt{\frac{(1 - m^2)\,(1 - m_s^2)\,r}{2\,E_s\,EI}}} \qquad (7)$$

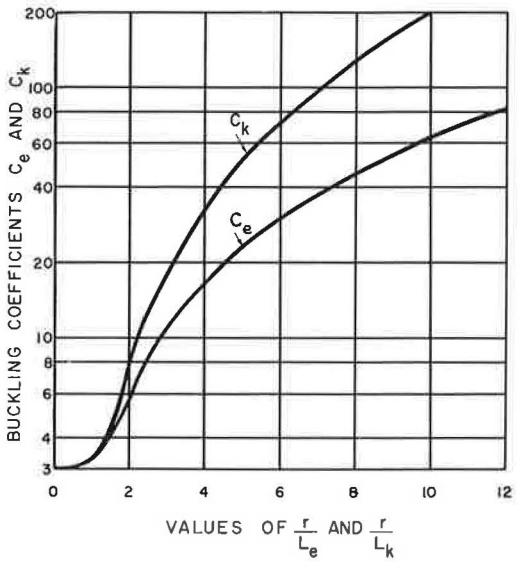


Figure 5. Theoretical buckling coefficients for circular culverts.

Eqs. 5 and 7 show that for good compaction of the backfill (when $r/L_e$ and $r/L_k$ exceed 2), the critical stress is practically independent of the radius of the culvert and the corresponding degree of compaction should increase with the radius. These equations have been plotted in Figure 6 for steel with E = 30,000,000 psi, $f_y$ = 40,000 psi and m = 0.3, by using the parameters of $\sqrt{\frac{A}{kI}}$ (Eq. 5) and $A\sqrt{\frac{r}{E_s I}}$ (Eq. 7). Both parameters give practically the same result so an average curve can be used for fills represented by either a coefficient of soil reaction k or a modulus of deformation $E_s$.

These expressions were derived for circular culverts with a uniform soil resistance and would, therefore, apply mainly to cover heights exceeding the culvert diameter for instance. The results can, however, also approximately be used for other cases, such as flexible arches with a shallow cover, by taking the effective radius of the section and average values for the height and soil properties of the cover. In order to apply the

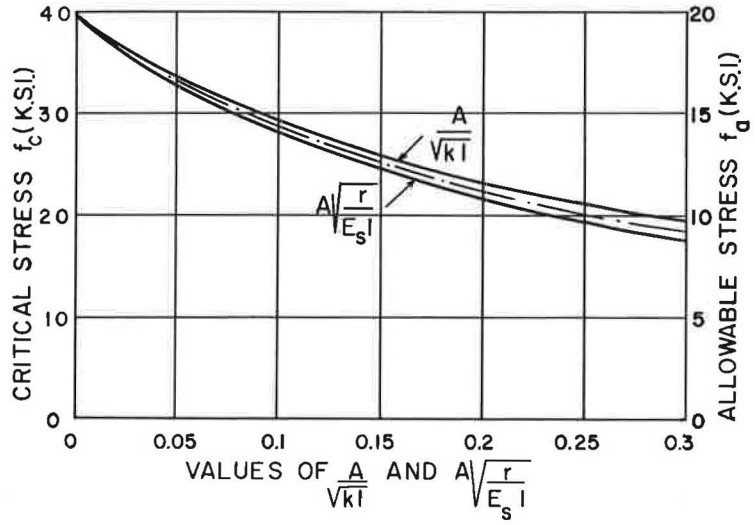


Figure 6. Theoretical critical and allowable stresses for steel culverts.

proposed analysis to an estimate of the critical stress governing the strength of flexible culverts in practice, the relevant physical properties of the culvert and fill have to be determined. Thus, the effective flexural rigidity EI of culverts should include the influence of flexibility of any joints, while the effective yield stress $f_y$ should be based on the culvert material or joint strength, whichever is least.

Regarding the properties of the fill, conservative values of the coefficient of soil reaction k or of the modulus of deformation $E_S$ should be chosen. The resistance of fills in the horizontal direction will usually govern in the case of sands and gravels. Thus, using an effective plate width of 1.5r causing buckling (see Appendix), the approximate effective coefficient of soil reaction (4) is as follows:

For clays

$$k = K_C/1.5r \tag{8}$$

For sands

$$k = K_S h/1.5r \tag{9}$$

in which

h = height of cover above culvert;
r = radius of culvert; and
$K_C$ and $K_S$ = constants of horizontal soil reaction for clays and sands, respectively.

Typical values of $K_C$ and $K_S$ (4) are given in Table 4. The values for sands apply to dry and moist materials and should be halved for submerged sands.

Moreover, the approximate modulus of deformation (4) is as follows:

For clays

$$E_S = K_C \tag{10}$$

For sands

$$E_S = K_S h \tag{11}$$

where the values of $K_C$ and $K_S$ are given in Table 4.

It is interesting to compare the values of the deformation properties of soils with the results of field observations on the deformation of flexible culverts under fills (7), summarized in Table 5. Using Eqs. 9 and 11 the analysis shows that the coefficient of soil reaction k and the modulus of deformation $E_S$ of loose fill are roughly one-half that of compact material, and the corresponding deduced values of the constant of soil reaction $K_S$ are also in good agreement with those given in Table 4. Moreover, for flexible culverts of average size (up to about 5-ft diameter) the coefficient of soil reaction k of the fill should not be less than about 20 pci, and greater values are suggested for larger structures. The corresponding modulus of deformation $E_S$ of the fill should not be less than about 1,000 psi, and for culvert diameters exceeding about 5 ft, the value of $E_S$ should increase roughly with the culvert diameter; about 200 psi per ft diameter.

These suggested values should be doubled for backfill near the structures, approximately, within a width of the culvert diameter which mainly affects their strength. The analysis of the field observations also shows that the ratio of $r/L_k$ (or $r/L_e$) varies from about 1.5 to 3.5. A value less than 2 should not be used in practice to insure that the critical stresses are sensibly independent of the culvert diameter, as shown by Eqs. 5 and 7. In that case, the maximum radial deflection d is also practically independent of the flexural rigidity of the culvert and can be estimated from the approximate relationships based on Spangler's formula (3)

TABLE 4

VALUES OF CONSTANT OF SOIL REACTION FOR CLAYS AND SANDS

| Clay | | Sand | |
|---|---|---|---|
| Consistency | Constant $K_c$ (psi) | Relative Density | Constant $K_s$ (pci) |
| Stiff | 500 - 1,000 | Loose | 1.5 - 4 |
| Very stiff | 1,000 - 2,000 | Compact (medium) | 4 - 12 |
| Hard | Over 2,000 | Dense | Over 12 |

TABLE 5

DEFORMATION PROPERTIES OF FILLS NEAR FLEXIBLE PIPE CULVERTS

| Location | Item No. | Soil Type (C. = compact, L. = loose) | Cover Hgt., h (ft) | Culvert Diameter, 2r (ft) | Coef. of Soil Reaction, k (pci) | Modulus of Deformation, $E_s$ (psi) | Constant of Soil Reaction, $K_s$ (pci) | Radius ÷ Rel. Stiff., $r/L_k$ |
|---|---|---|---|---|---|---|---|---|
| Ames, Iowa | 1 | L. loam | 15 | 3.5 | 14 | 440 | 2.4 | 2.4 |
| | 2 | L. gravel | 16 | 3.5 | 32 | 1,020 | 5.3 | 2.9 |
| | 3 | C. sand-clay | 15 | 3.0 | 28 | 755 | 4.2 | 2.6 |
| | 4 | L. sand-clay | 15 | 3.0 | 13 | 350 | 1.9 | 2.2 |
| | 5 | C. sand-clay | 15 | 3.5 | 25 | 790 | 4.4 | 2.8 |
| | 6 | L. sand-clay | 15 | 3.5 | 15 | 470 | 2.6 | 2.4 |
| | 7 | C. sand-clay | 15 | 4.0 | 29 | 1,040 | 5.8 | 3.4 |
| | 8 | L. sand-clay | 15 | 4.0 | 14 | 505 | 2.8 | 2.8 |
| | 9 | C. sand-clay | 15 | 5.0 | 26 | 1,170 | 6.5 | 3.6 |
| | 10 | L. sand-clay | 15 | 5.0 | 12 | 540 | 3.0 | 3.0 |
| Chapel Hill, N.C. | 11 | Sand | 12 | 2.5 | 25 | 560 | 3.9 | 1.8 |
| | 12 | Sand | 12 | 2.6 | 56 | 1,320 | 9.2 | 2.3 |
| | 13 | Sand | 12 | 2.5 | 80 | 1,800 | 12.5 | 2.5 |
| | 14 | Sand | 12 | 1.7 | 35 | 525 | 3.7 | 1.3 |
| | 15 | Sand | 12 | 1.8 | 82 | 1,290 | 9.0 | 1.7 |
| Culman, Ala. | 16 | C. crushed rock | 137 | 7.0 | 190 | 12,000 | 7.3 | 3.2 |
| McDowell, N.C. | 17 | C. sandy silt | 170 | 5.5 | 40 | 1,980 | 1.4 | 1.7 |
| Denver, Colo. | 18 | Crushed rock | 41 | 15.0 | 10 | 1,350 | 2.7 | 2.9 |
| Colorado | 19 | L. silty sand | 13 | 10.0 | 4 | 360 | 2.3 | 1.7 |

$$d = 2.7\, p/k \tag{12}$$

or, substituting Eqs. 8 to 11,

$$d = 4\, p r/E_s \tag{13}$$

where p = average vertical soil pressure on culvert, and other symbols as before.

After the critical stress $f_c$ of culverts has been estimated (Eq. 5 or 7), a safety factor of at least 2 should be used to determine the allowable axial stress $f_a$, as shown in Figure 6. The culvert can then readily be designed by the simple ring compression theory (Eq. 1), and the maximum deflection can be estimated (Eq. 12 or 13) to check that both the strength and deformation of the culvert are within permissible limits.

In the absence of published field data on the buckling of flexible culverts, the proposed analysis can be applied to a series of model loading tests by Watkins (6). In these tests plain steel culverts of about 2-in. diameter were embedded in a container filled with sand of various densities and they were loaded to failure by a vertical pressure applied to the ground surface. Using Spangler's formula of the deflection of flexible culverts (3), the coefficients of soil reaction k have been deduced from the experimental load-deflection curves, which were roughly linear until failure of the culverts. Substituting these values into Eq. 5, the theoretical soil pressures producing buckling failure of the culverts are found to be in good agreement with the observed values, if the yield stress is deduced from tests on culverts in very dense material when failure occurred by crushing of the material (Table 6).

TABLE 6

RESULTS OF LOADING TESTS ON MODEL CULVERTS BY WATKINS (6)

| Item No. | Coef. of Soil Reaction, k (pci) | Critical Soil Pressure[a] | | | |
|---|---|---|---|---|---|
| | | t = 0.04 in. | | t = 0.01 in. | |
| | | Observed (psi) | Theoret. (psi) | Observed (psi) | Theoret. (psi) |
| 1 | 30,000 | 410 | C[a] | 175 | C[a] |
| 2 | 12,000 | 340 | 350 | 125 | 125 |
| 3 | 4,000 | 300 | 320 | 115 | 105 |
| 4 | 2,000 | 270 | 290 | 90 | 90 |
| 5 | 1,000 | 220 | 250 | 85 | 75 |

[a] t = culvert thickness; C = crushing failure.

Although further evidence, especially from full-scale observations of the ultimate strength of flexible culverts under various soil conditions is desirable, it may be concluded that the proposed method of analysis can be used to estimate the strength of culverts under fills in practice.

## CONCLUSIONS

1. A series of model tests on plain and corrugated steel culvert sheets bearing against dense sand, as well as some earlier tests on model culverts, shows that for small values of the coefficient of soil reaction or modulus of deformation of the backfill, and for small values of the flexural rigidity of the sheets, failure occurs by buckling. However, for large values of these parameters, failure occurs by yielding of the section.
2. The theory of elastic stability of plates has been extended to estimate the critical buckling stresses of circular sheets and culverts in an elastic medium, and simple equations and design charts are presented for use in practice.
3. To insure that the critical stresses in flexible culverts are sensibly independent of the culvert diameter, minimum values of the coefficient of soil reaction and modulus of deformation of fills have been suggested from an analysis of the deformation of culverts under fills in practice.
4. The results of the present model tests on circular sheets, and earlier experiments with model culverts, support the proposed method of analysis which can be used in conjunction with the ring compression theory to estimate the strength of flexible culverts under fills.
5. It is hoped that field observations will be made on the ultimate strength of culverts under various soil conditions for comparison with the proposed method of analysis.

## ACKNOWLEDGMENT

The authors are indebted to the National Corrugated Metal Pipe Association for encouragement and support and many helpful discussions with C. L. Fisher and H. L. White of Armco Drainage and Metal Products, Inc. The junior author is also grateful for a Bursary of the National Research Council of Canada.

## REFERENCES

1. Baikie, L. D., "Strength of Curved Plates Bearing Against Dense Sand." Unpublished M. E. thesis, Nova Scotia Technical College, Halifax, N. S. (1961).
2. Meyerhof, G. G., "An Investigation of the Bearing Capacity of Shallow Footings on Dry Sand." Proc. 2nd Int. Conf. Soil Mechanics, Vol. 1, p. 237 (1948).
3. Spangler, M. G., "The Structural Design of Flexible Pipe Culverts." Public Roads, Vol. 18, p. 217 (1938).
4. Terzaghi, K., "Evaluation of Coefficient of Subgrade Reaction." Geotechnique, Vol. 5, p. 297 (1955).
5. Timoshenko, S. P., and Gere, J. M., "Theory of Elastic Stability." McGraw-Hill, New York (1961).
6. Watkins, R. K., "Failure Conditions of Flexible Culverts Embedded in Soil." HRB Proc., 39:361-371 (1960).
7. Watkins, R. K., and Spangler, M. G., "Some Characteristics of the Modulus of Passive Resistance of Soil: A Study in Similitude." HRB Proc., 37: 576-583 (1958).
8. White, H. A., and Layer, J. P., "The Corrugated Metal Conduit as a Compression Ring." HRB Proc., 39:389-397 (1960).

# *Appendix*

## NOTATION

$a$ = length of plate;
$A$ = cross-sectional area of plate;
$b$ = width of plate;
$C$, $C_e$, $C_k$ = buckling coefficients of plate or culverts;
$d$ = radial deflection of plate or culvert;
$E$ = modulus of elasticity of plate or culvert;
$E_s$ = modulus of deformation of soil;
$f$ = unit stress in plate;
$f_a$ = axial stress in plate or culvert;
$f_b$ = buckling stress of plate or culvert;
$f_c$ = critical stress in plate or culvert;
$f_y$ = yield stress of plate or culvert;
$h$ = height of cover above culvert;
$I$ = moment of inertia per unit width of plate or unit length of culvert;
$k$ = coefficient of soil reaction ("subgrade modulus");
$K_c$, $K_s$ = constants of soil reaction;
$L_e$, $L_k$ = relative stiffness of plate or culvert with respect to soil;
$m$ = Poisson's ratio of plate;
$m_s$ = Poisson's ratio of soil;
$n$ = number of half-waves or order of buckling modes;
$p$ = soil pressure on plate or culvert;
$P_b$ = buckling force per unit width of plate or unit length of culvert;
$r$ = radius of plate or culvert;
$t$ = thickness of plate or culvert;
$\theta$ = center angle of half-wave.

## BUCKLING OF CIRCULAR PLATES AND CULVERTS IN ELASTIC MEDIUM

If a long flat plate is supported by an elastic medium of which the reaction pressure at any point is directly proportional to the deflection and the plate is compressed by a uniformly distributed axial force acting along hinged edges, it can be shown (5) that the critical buckling force per unit width of the edge is

$$P_b = \frac{\pi^2 E I}{(1 - m^2)\, a^2}\left[ n^2 + \frac{(1 - m^2)\, k\, a^4}{n^2 \pi^4 E I} \right] \tag{14}$$

The value of n can be determined from the relationship

$$n^2 (n + 1)^2 = \frac{k\, a^4 (1 - m^2)}{n^4 E I} \tag{15}$$

As k increases, the number of half-waves increases, and for a large number of waves, the critical buckling force is independent of the length of the plate and is

$$P_b = 2\sqrt{\frac{k E I}{1 - m^2}} \tag{16}$$

A rigorous analysis of the buckling of cylindrical plates supported by an elastic medium is not yet available. However, an approximate solution can be obtained by combining the above results for flat plates with the analysis of the buckling of cylindrical plates under uniform external pressure for which the critical buckling force per unit width of the edge is (5)

$$P_b = \frac{EI}{(1-m^2)r^2}\left(\frac{\pi^2}{\theta^2} - 1\right) \tag{17}$$

or

$$P_b = \frac{\pi^2 EI}{(1-m^2)a^2}\left(1 - \frac{\theta^2}{\pi^2}\right) \tag{18}$$

in which

a = arc length of half-wave, and other symbols are given in the notation.

Eq. 18 shows that for $\theta = 90^0$, which represents a quadrantal cylindrical plate and the lowest buckling mode of a circular culvert, the buckling force is three-quarters that of a freely supported flat plate (Eq. 14 for k = 0 and n = 1). As the angle $\theta$ decreases and the number of half-waves n increases, Eq. 18 rapidly approaches the corresponding value for a flat plate. Thus, for a circular culvert under an external pressure, Eq. 17 can be rewritten as

$$P_b = \frac{[(n+1)^2 - 1]\,EI}{(1-m^2)r^2} \tag{19}$$

If the radial deflection curve of a half-wave of a cylindrical plate in an elastic medium compressed by a uniformly distributed axial force acting along hinged edges is assumed to be the same as that for a similar flat plate, the critical buckling force of a cylindrical plate will approach that of a flat plate as n increases. Thus, by substituting Eq. 19 into Eq. 14 the critical buckling force per unit length of a circular culvert in an elastic medium may be represented by

$$P_b = \frac{EI}{(1-m^2)r^2}\left[(n+1)^2 - 1 + \frac{(1-m^2)kr^4}{[(n+1)^2 - 1]\,EI}\right] \tag{20}$$

in which the term in large square brackets represents the buckling coefficient C. This coefficient, which is similar to that of a flat plate, can be evaluated in the same manner (see Eq. 15) and is shown in Figure 5 in terms of the ratio $r/L_k$, where

$$L_k = \sqrt[4]{\frac{EI}{(1-m^2)k}} \tag{21}$$

For the fundamental buckling mode with n = 1, the buckling coefficient from Eqs. 20 and 21 is

$$C_k = 3 + \tfrac{1}{3}(r/L_k)^4 \tag{22}$$

which holds, approximately, for $r/L_k < 2$, while for higher buckling modes the buckling coefficient is nearly

$$C_k = 2\,(r/L_k)^2 \tag{23}$$

for $r/L_k > 2$.

Substituting Eq. 23 into Eq. 20 the critical buckling force for $r/L_k > 2$ is

$$P_b = 2\sqrt{\frac{k\,E\,I}{1 - m^2}} \tag{24}$$

and the corresponding buckling stress is

$$f_b = \frac{2}{A}\sqrt{\frac{k\,E\,I}{1 - m^2}} \tag{25}$$

as for flat plates and with the upper limit of the yield stress $f_y$ of the plate.

Frequently the deformation properties of the elastic medium can be represented by a modulus of deformation $E_s$ and Poisson's ratio $m_s$. In that case the above equations can be adapted by using the approximate relationship (4)

$$k = E_s/b \tag{26}$$

where b governs the deflection at the critical load. Thus, conservative estimates will be obtained by using b = a for flat plates and b = 1.5r for circular culverts when

$$k = E_s/1.5r \tag{27}$$

or

$$k = \frac{E_s}{2\,(1 - m_s^2)\,r} \tag{28}$$

because Poisson's ratio $m_s = \frac{1}{2}$, approximately.

Substituting Eq. 28 into Eq. 20 the critical buckling force is

$$P_b = \frac{E\,I}{(1 - m^2)\,r^2}\left[(n+1)^2 - 1 + \frac{(1 - m^2)\,E_s\,r^3}{2\,[(n+1)^2 - 1]\,(1 - m_s^2)\,E\,I}\right] \tag{29}$$

where the term in large square brackets represents the corresponding buckling coefficient $C_e$. This coefficient has been so evaluated and is shown in Figure 5 in terms of the ratio $r/L_e$, where the relative stiffness

$$L_e = \sqrt[3]{\frac{2(1 - m_s^2)\,E\,I}{(1 - m^2)\,E_s}} \tag{30}$$

Further, proceeding as before,

$$C_e = 3 + \tfrac{1}{3}\,(r/L_e)^3 \tag{31}$$

for $r/L_e < 2$, and approximately,

$$C_e = 2(r/L_e)^{3/2} \tag{32}$$

for $r/L_e > 2$ when the critical buckling force becomes

$$P_b = \sqrt{\frac{2\,E_s\,E\,I}{(1 - m^2)(1 - m_s^2)\,r}} \tag{33}$$

for $r/L_e > 2$.

In order to make some allowance for accidental eccentricities and imperfections of the culvert, the critical stress can conveniently be expressed by (5)

$$f_c = \frac{f_y}{1 + f_y/f_b} \tag{34}$$

Thus, substituting Eq. 20 into Eq. 34 the critical stress is

$$f_c = \frac{f_y}{1 + \dfrac{f_y (1 - m^2) A r^2}{C E I}} \tag{35}$$

or, using Eqs. 25 and 33,

$$f_c = \frac{f_y}{1 + \dfrac{f_y A}{2} \sqrt{\dfrac{1 - m^2}{k E I}}} \tag{36}$$

for $r/L_k > 2$, and

$$f_c = \frac{f_y}{1 + f_y A \sqrt{\dfrac{(1 - m^2)(1 - m_s^2) r}{2 E_s E I}}} \tag{37}$$

for $r/L_e > 2$.

## *Discussion*

REYNOLD K. WATKINS, Professor and Head, Department of Mechanical Engineering, Utah State University—Dr. Meyerhof and Mr. Baikie have reported an important aspect of the structural performance of buried flexible conduits; namely, the interaction of ring crushing and hydrostatic buckling.

This discussion (a) encourages use of a column analogy for presentation of Meyerhof and Baikie's results; (b) provides a model study check for their concepts; (c) suggests a limit for conduit ring design if soil is poor and/or the installation is not well controlled; and (d) indicates areas for much needed additional study.

Model studies conducted at Utah State University are the prime source of the information and methods of presentation reported herein. Notation is as in Figure 7.

As a basis for design, ring failure is defined from observations on model tests (Fig. 8) to be either:

1. Deflection: (a) greater than some maximum permissible for adequate conduction and/or (b) causing excessive soil displacement; or
2. Buckling: (a) ring crushing (inelastic buckling); and/or (b) hydrostatic buckling (elastic buckling).

Deflection failure of the flexible conduit ring can be predicted by a method proposed by Spangler (9). Deflection $\Delta X/D$ for a given height of fill or vertical soil pressure p may be controlled partly by the conduit flexibility $D^3/EI$, and partly by the soil properties $E'$ (soil type, moisture content, soil density, etc.).

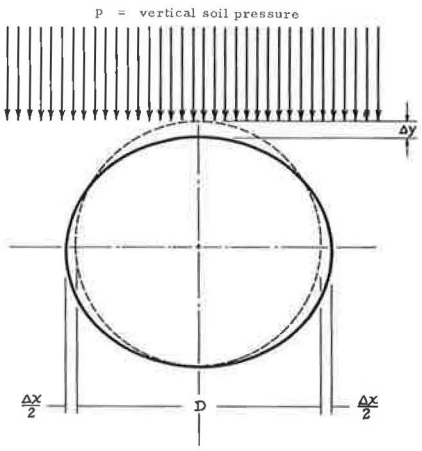


NOTATION

EI = ring wall stiffness per unit length of conduit, in kip-in.;
A = cross-sectional area of wall per unit length, in sq in.;
E' = soil modulus (corresponds to modulus of elasticity for elastic materials), in kips per sq in.;
$D^3/EI$ = conduit ring flexibility, in sq in. per kip;
$f_c$ = ring compression stress in conduit wall, in kips per sq in.;
$f_y$ = yield stress, in kips per sq in.;
k = radius of gyration of wall cross-section, in in.; and
SF = safety factor.

Figure 7. Notation associated with the performance of buried flexible conduit.

Design by deflection will not be considered further in this discussion; however, it may not be disregarded. Model studies prove that failure can indeed occur by excessive deflection.

Figure 8 also shows a typical buckling failure as observed in model studies. White (8) has suggested that this type of failure is due to ring compression or crushing of the conduit wall (inelastic buckling). The design equation is

$$\frac{pD}{2A} = \frac{f_y}{SF} \qquad (38)$$

Buckling failure has also been considered in terms of collapse due to a critical external hydrostatic pressure (elastic buckling). Brockenbrough (10) suggests the hydrostatic buckling equation

$$p\,\frac{D^3}{EI} = \frac{24}{SF} \qquad (39)$$

as a conservative design limit except when ring compression controls. When does ring compression control, and when does hydrostatic buckling control? Is there an interaction of both effects calling for a further reduced design limit?

Interaction is suspected if one compares conduit strength with the strength of a column. A short heavy column having very low slenderness fails in crushing (Fig. 9). This is inelastic buckling. If the column is long and very slender, buckling failure will occur according to the Euler equation. This is elastic buckling. However, column tests show that there is an interaction range in which column strengths fall below both crushing and buckling.

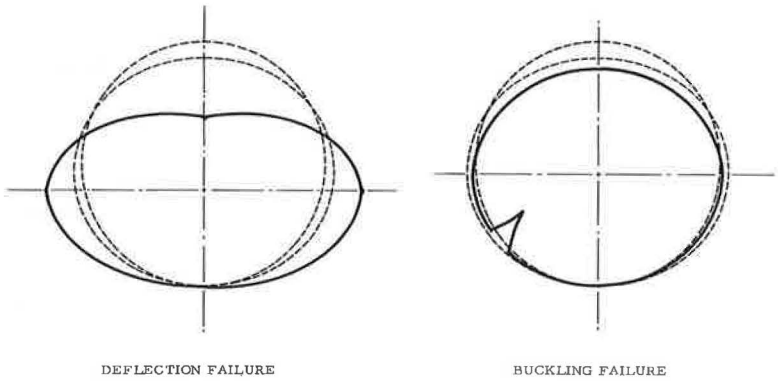


Figure 8. Two general types of structural ring failure of buried flexible conduits observed from model studies.

By analogous reasoning, ring buckling strength may be plotted for buried flexible conduits (Fig. 10). Therefore,

$$\frac{1}{E}\left(\frac{D}{k}\right)^2 = \frac{D^3}{EI}\left(\frac{A}{D}\right) \tag{40}$$

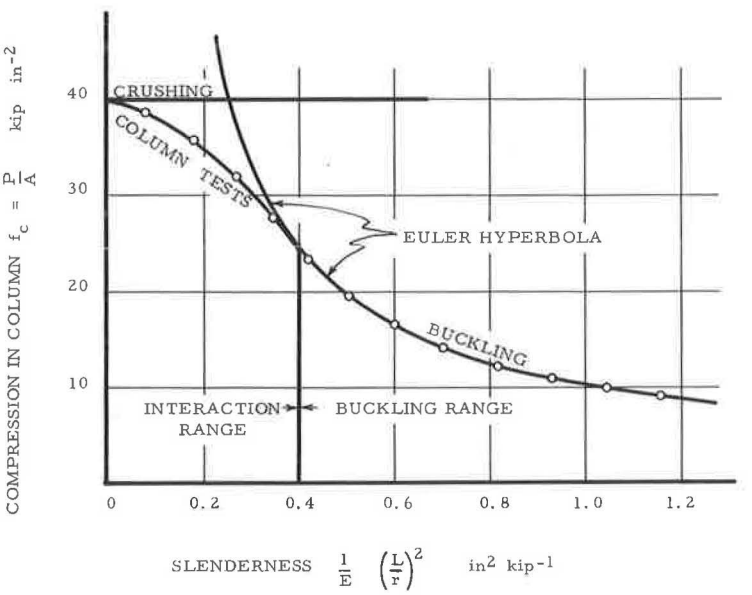


Figure 9. Typical presentation of column strength curves.

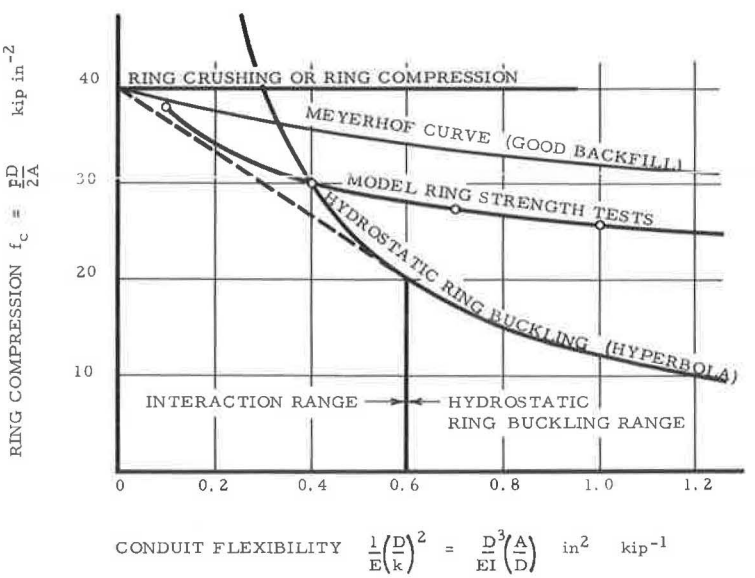


Figure 10. Ring buckling strength curves for buried flexible conduits.

TABLE 7

ALLOWABLE HEIGHT OF SOIL FILL IN FEET ABOVE TOP OF BURIED FLEXIBLE STEEL CONDUIT

Corrugation Configuration { 1/2 × 2 2/3

| Diam. (in.) | Gage | | | | | | | | | | |
|---|---|---|---|---|---|---|---|---|---|---|---|
| | 10 | 12 | 14 | 16 | 18 | 20 | 22 | 24 | 26 | 28 | 29 |
| 12 | 515 | 400 | 287 | 228 | 183 | 137 | 114 | 91 | 68 | 57 | 52 |
| 15 | 397 | 298 | 214 | 171 | 137 | 105 | 86 | 67 | 52 | 42 | 38 |
| 18 | 292 | 227 | 162 | 129 | 104 | 78 | 65 | 52 | 38 | 32 | 29 |
| 21 | 222 | 172 | 123 | 98 | 79 | 59 | 49 | 39 | 29 | 24 | 22 |
| 24 | 165 | 129 | 92 | 73 | 59 | 44 | 36 | 29 | 21 | 18 | 16 |
| 30 | 86 | 67 | 48 | 38 | 31 | 23 | 19 | 15 | 11 | 8 | 5 |
| 36 | 50 | 39 | 27 | 22 | 17 | 13 | 10 | 6 | | | |
| 42 | 32 | 25 | 18 | 14 | 10 | 5 | | | | | |
| 48 | 21 | 17 | 12 | 6 | | | | | | | |
| 54 | 14 | 10 | | | | | | | | | |
| 60 | 9 | | | | | | | | | | |

Corrugation Configuration { 1 × 3

| Diam. (in.) | Gage | | | | | | | | | | |
|---|---|---|---|---|---|---|---|---|---|---|---|
| | 10 | 12 | 14 | 16 | 18 | 20 | 22 | 24 | 26 | 28 | 29 |
| 12 | 644 | 501 | 358 | 285 | 226 | 169 | 143 | 115 | 85 | 73 | 65 |
| 15 | 505 | 393 | 281 | 224 | 178 | 133 | 112 | 91 | 66 | 57 | 51 |
| 18 | 412 | 322 | 230 | 183 | 146 | 109 | 91 | 74 | 54 | 46 | 41 |
| 21 | 347 | 270 | 192 | 153 | 122 | 91 | 77 | 62 | 45 | 39 | 35 |
| 24 | 294 | 219 | 164 | 130 | 104 | 77 | 65 | 53 | 38 | 33 | 29 |
| 30 | 219 | 171 | 122 | 97 | 77 | 58 | 48 | 39 | 28 | 24 | 22 |
| 36 | 163 | 127 | 91 | 72 | 58 | 43 | 36 | 29 | 21 | 18 | 16 |
| 42 | 123 | 96 | 68 | 54 | 43 | 32 | 27 | 21 | 15 | 13 | 11 |
| 48 | 90 | 70 | 50 | 40 | 32 | 23 | 19 | 15 | 11 | 8 | 6 |
| 54 | 65 | 50 | 35 | 27 | 22 | 16 | 13 | 10 | | | |
| 60 | 47 | 36 | 25 | 21 | 16 | 11 | 9 | | | | |
| 66 | 35 | 27 | 19 | 15 | 11 | 6 | | | | | |
| 72 | 27 | 20 | 14 | 11 | 7 | | | | | | |
| 78 | 21 | 16 | 11 | 7 | | | | | | | |
| 84 | 16 | 12 | 7 | | | | | | | | |
| 90 | 13 | 9 | | | | | | | | | |
| 96 | 10 | 6 | | | | | | | | | |

Design Assumptions:

1. Safety factor = 2. Allowable height of fill is approximately inversely proportional to the safety factor; e.g., the fill heights listed above must be reduced by half for a safety factor of 4.
2. Unit weight of soil is 100 pcf and H-20 liveload is on the surface.
3. Modulus of elasticity for the steel conduits is 33 kips per sq in.
4. Deflection must be checked.

where $D^3/EI$ is the conduit ring flexibility on which the hydrostatic buckling formula is based.

The ring compression equation plots as a horizontal ring crushing line like the crushing line for a column. The hydrostatic buckling equation plots as a hyperbola like the Euler column formula for buckling. Like actual column tests, a series of model tests falls below both curves within an interaction range. This substantiates the authors' conclusion that ring compression and hydrostatic buckling interact. It is here suggested that diagrams like Figure 10 be used to present this interaction concept.

The model test curve of Figure 10 rises above the hydrostatic buckling curve as conduit flexibility increases. This is because the soil was not hydrostatic. Actually the soil developed some strength and partially supported the ring. Conduit strength curves for highly plastic soil (hydrostatic) approach the hydrostatic buckling curve. Plots for dense, angular, non-plastic soil approach the ring compression line. The quality of the soil around the conduit determines where the conduit strength curve falls between these two extremes. If the backfill is good and conduit flexibility is low (i.e., if the conduit shape is not altered during loading) the ring compression theory may be an adequate basis for design. However, for questionable backfill and/or high conduit flexibility, the hydrostatic buckling theory is safer. Additional experimental work is needed to determine where the strength curve will fall between these two extremes, depending on soil properties.

Until such work is done, it is recommended that for average installations, conduit strength be conservatively defined as shown by the dashed line in the interaction range and the hydrostatic hyperbola in the hydrostatic ring buckling range.

In these model tests the observed yield point is 40 kips per sq in. In actual installations the yield point may be different depending on the material. For example, a conservative yield point for corrugated culvert steel is 33 kips per sq in. The equation for design strength in the interaction range is then

$$\frac{pD}{2A} = \left[33\text{ksi} - \frac{363}{16}\,\frac{D^3}{EI}\,\left(\frac{A}{D}\right)\right] \div SF \qquad (41)$$

for values of $D^3/EI\,(A/D)$ less than 0.72 sq in. per kip.

Above this value the design strength is given by Eq. 39. For those who prefer design tables, this could be recorded in a form of Table 7. If such tables are not published, it would be convenient to publish the values $D^3/EI$ and $D/A$ for use in design equations. Table 7 is based on a safety factor of 2. Using such conservative design limits there is no apparent need for a greater safety factor for average installations. The height of fill is based on an assumed unit weight of soil of 100 pcf with an H-20 live load. Information on conduit deflection should accompany any published design data.

Table 7 includes some height of fill values for a proposed deeper corrugation referred to as a 1 x 3 corrugation. The deeper corrugation has better resistance to buckling.

It is recommended that the effect of soil properties on conduit buckling be investigated. Conduit deflection at buckling failure should be investigated for various soil-conduit systems. The adequacy of the vertical soil pressure p as used in the design formulas should be checked.

## REFERENCES

9. Spangler, M. G., "Soil Engineering." Internat. Textbook Co., Scranton, Pa., p. 433 (1960).
10. Brockenbrough, R. L., "A Theoretical Evaluation of Two Corrugation Profiles for Corrugated Metal Pipe Culverts." Memorandum, U. S. Steel Corp., ARL Proj. 90.12-017 (Feb. 1962).

G. G. MEYERHOF and L. D. BAIKIE, Closure—The authors are grateful to Professor Watkins for his interesting contribution to the discussion and they agree that the column analogy would provide a good basis for the presentation of their test results on the strength of steel culvert sheets. This is shown by a comparison of the observed maximum axial stress with the theoretical critical stress of the sheets at failure given in Table 3, although the range of relative stiffnesses of the sheets to the soil or the "conduit flexibility" was rather limited. A wider range of conduit flexibilities was studied by Professor Watkins in his series of model tests, which also support the authors' analysis, as shown in Table 6.

The model test curve (Fig. 10) compares well with the theoretical interaction relationship between ring crushing and buckling, as expressed by Eq. 3 if the buckling coefficient C is taken to be about 15. This value is 5 times the hydrostatic buckling coefficient of 3 and represents a high degree of compaction of the sand in the model tests. Even for average installations when the ratio of culvert radius to relative stiffness (r/L) is about 2, the theoretical buckling coefficient would be about 2 to 3 times the hydrostatic value (Fig. 5). The corresponding design curves in Figure 6 can then be used to estimate the strength of steel culverts in terms of their stiffness (or "flexibility") as well as the deformation (or "strength") properties of the soil. On the other hand, the authors believe that Eq. 41 and Table 7 proposed on the basis of hydrostatic ring buckling would give unduly conservative estimates in practice.

# Load Testing of No-Joint Cast-in-Place Concrete Pipe

A. MORGAN JOHNSON, Assistant City Engineer, Phoenix, Arizona; and JOHN D. HESS, President, Phoenix Testing Laboratories

The city of Phoenix, city engineer's office, during the summer of 1961 drew up a research program of load testing of cast-in-place concrete pipe, using SR-4 strain gages. A 48-in. cast-in-place no-joint pipe was installed under usual field conditions and close inspection, using specifications of the Bureau of Reclamation and of the city of Phoenix. The installation was divided into four 25-ft test sections, which were tested in turn under 24, 18, 12, and 6 in. of compacted granular backfill. Loads were applied as static axle loads, varying from 10,000 to 36,000 lb. Strains were observed, along with changes in diameter, changes in elevation of the pipe, and soil pressures.

Visual observations indicated no distress to the pipe under the most extreme loading conditions. Changes in horizontal and vertical diameter were negligible, and there was no appreciable settlement of the pipe. By a series of tests on the concrete, attempts were made to establish stress-strain relationships in the concrete used. Results obtained were not conclusive but interesting data were obtained. Further work of this type is needed to establish relationships between observed strains and stresses in the concrete and the theories of structural design and analysis for pipe of this sort.

• IN its program of improving major arterial and collector streets, the city of Phoenix is frequently faced with the problem of enclosing (or tiling) an irrigation ditch. The water in these ditches is the "life blood" of the Phoenix area and its flow must be preserved at all cost. The Salt River Valley Water Users Association, which handles the irrigation water has an extensive network of laterals on the section-line and quarter-line roads. These irrigation ditches exist under rights which are prior to those of the establishment of the roads themselves and consequently it is the responsibility of the city, under its paving programs, to tile the ditches or to relocate them off the traveled roadway. Inasmuch as the development of the area is greatly enhanced by putting the lines underground, the city has adopted a program of enclosing them rather than simply relocating.

The Salt River Project has its own equipment for pouring continuous, cast-in-place, no-joint concrete pipe and has used this process for many miles of line which have been constructed on Project right-of-way. The city was faced with the necessity of approving or disapproving this type of construction when constructed in street right-of-way by or for the Project forces. The Project engineers had been working for some time to establish the adequacy of cast-in-place pipe for use as irrigation lines under traveled roadways and to obtain approval of the Bureau of Reclamation for this type of installation. It was granted with a minimum cover of 24 in. on lightly traveled roadways and 30 in. on heavily traveled roadways.

Paper sponsored by Committee on Culverts and Culvert Pipe.

Consequently, Phoenix became interested in the possibility of using this continuous-pour pipe on its own projects where irrigation lines were involved. It was also desired to determine the acceptability of cast-in-place pipe as an alternate material on storm drain construction.

Two distinguishing features of cast-in-place pipe are (a) the trench is cut to serve as the outside form of the lower portion of the pipe, and (b) the pipe is actually formed directly in the trench. The trench is shaped to a semicircular bottom, equal in radius to the outside radius of the pipe and the sides are generally vertical above the springline. A "boat" which advances along the trench provides slip forms for the pipe invert and for the upper portion of the outer surface. The arch of the pipe is supported by collapsible aluminum forms or other methods. A low-slump concrete is fed from a hopper, and around the forms. This process results in complete bedding condition for the pipe up to and above the springline. Figure 1 shows the typical shape of the cross-section. The concrete develops sufficient strength so that the forms are usually removed prior to the start of the following day's pour.

The city engineer's office reviewed the available information on cast-in-place pipe and determined to obtain further knowledge of its properties by actual test loading of a typical installation. A cooperative research program was worked out, using personnel of the city, facilities of the Salt River Project, and an installation furnished by the manufacturer's representative. Instrumentation was performed by Phoenix Testing Laboratories. The objectives of the program were as follows:

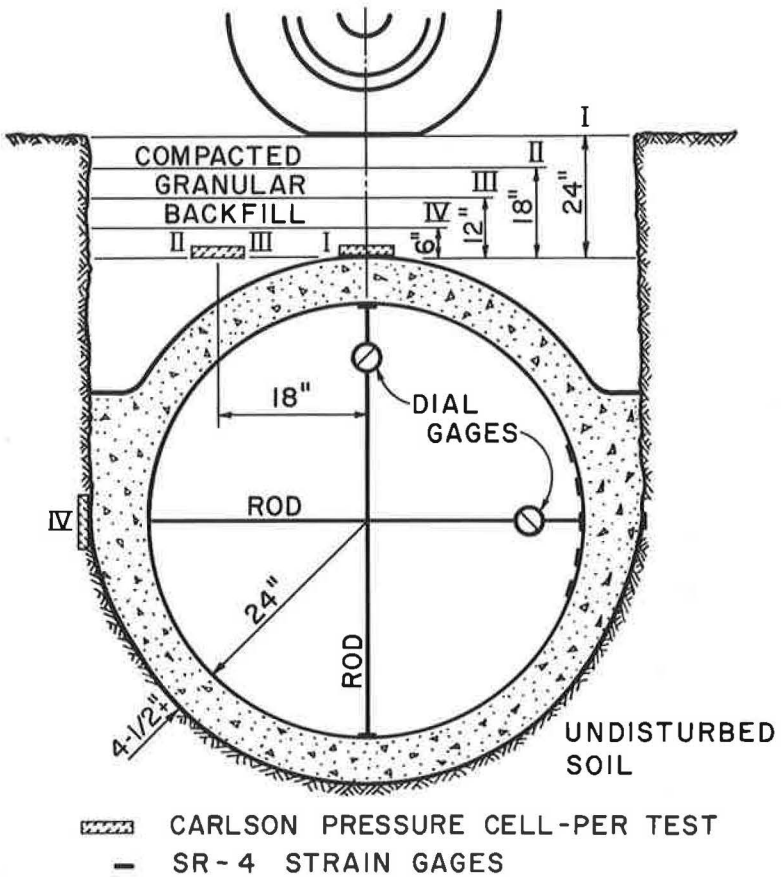


Figure 1. Schematic cross-section.

1. To serve as a pilot program to establish the methods of procedure;
2. To determine the type of stress information which might be obtained under static axle loads;
3. To observe the action of the pipe under heavy axle loads with shallow cover; and
4. To provide data for planning a more extensive investigation.

The application of structural theory (such as arch analysis or the ring concept) to cast-in-place pipe, while valuable, involves assumptions whose validity has been questioned. It was felt that a direct measurement of strains under loading would provide the best indication of the ability of the pipe to carry actual loads. Relationships between strain and stress could be established and stresses thus determined could be compared with the fatigue limit of the concrete and with corresponding design stresses under repeated loading. The controlled installation was proposed because of the difficulty of controlling traffic on an established roadway and the impracticability of determining actual loads of free traffic.

## GENERAL METHOD OF TEST

The approach proposed for determining the load-carrying capacity of cast-in-place concrete pipe was one of measurement of strains, following a controlled construction condition, and under controlled axle loads. The pipe was constructed and backfilled under close inspections conforming to Bureau of Reclamation and city specifications. Known axle loads were applied to the surface above the pipe and strains at critical points were observed with SR-4 strain gages attached to the pipe. The stress-strain properties of the concrete were studied and correlated with tests on cylinders, beams and cores, and estimations of the fatigue limit and modulus of elasticity were made. These data were expected to lead to an evaluation of the safe load design for the pipe under the various test conditions.

## FIELD INSTALLATION

### Soil Investigations

Prior to construction, soil investigations were made along the axis of the proposed installation to establish the fact that the site chosen was not untypical of Phoenix conditions. Classification tests were run on the samples thus obtained and results are given in Table 1.

Following the digging of the trench, samples were taken of the undisturbed material at the bottom and sides of the trench to determine in-place native density and moisture content. These typical results are given in Table 2. Gradation and Atterburg Limits of these samples were correlated with those shown in Table 1.

Proposed backfill material was tested for conformance with city specifications and moisture-density curves were run. Characteristic properties of these materials are given in Tables 3 and 4.

### Pipe Construction

A 100-ft run of 48-in. cast-in-place concrete pipe was constructed. Average pipe thickness was $4\frac{1}{2}$ in. and the invert was located about 6 ft below the surrounding

TABLE 1

AVERAGE PROPERTIES OF NATIVE SOIL

| Location | Depth (ft) | T-99 | | LL | PI | % Passing | | | HRB Soil Class. |
|---|---|---|---|---|---|---|---|---|---|
| | | Max. Density (pcf) | Optimum M. C. (%) | | | #200 | 0.05mm | 0.005mm | |
| Sta. 0 to 1+00 | 0 to 3 | — | — | 28 | 7 | 52 | 38 | 7 | A-4 |
| Sta. 0 to 1+00 | 3 to 5.5 | 115 | 14 | 35 | 13 | 52 | 38 | 7 | A-6 |
| Sta. 0 to 1+00 | 5.5 to 8 | — | — | 35 | 13 | 52 | 38 | 7 | A-6 |
| Open ditch | Bottom | 105 | 19 | 57 | 19 | 46 | 25 | 5 | A-7 |
| Open ditch | Springline | 115 | 14 | 35 | 9 | 47 | 35 | 7 | A-4 |

TABLE 2

DENSITY OF NATIVE SOIL IN TRENCH

| Location | Depth | T-99 Density (pcf) | Optimum Moisture (%) | Native Density (pcf) | Percent T-99 Density | Native Moisture (%) |
|---|---|---|---|---|---|---|
| Sta. 0+15.5 | Bottom | 105 | 19 | 75.6 | 72 | 10.0 |
| Sta. 0+40.5 | Bottom | 105 | 19 | 79.8 | 76 | 11.0 |
| Sta. 0+65.5 | Bottom | 105 | 19 | 84.0 | 80 | 10.4 |
| Sta. 0+90.5 | Bottom | 105 | 19 | 84.0 | 80 | 11.0 |
| Sta. 0+15.5 | Springline | 110 | 16 | 83.5 | 76 | 14.4 |
| Sta. 0+40.5 | Springline | 115 | 14 | 90.9 | 79 | 15.5 |
| Sta. 0+65.5 | Springline | 115 | 14 | 83.6 | 77 | 15.0 |

ground. The shaped trench was cut the day before casting the pipe. The sides and bottom of the trench were sprayed with water prior to casting to reduce moisture loss from the fresh concrete. Personnel of the Phoenix office of the Bureau of Reclamation closely observed the installation and pronounced it a good typical installation.

The 100-ft stretch was designed as four 25-ft test sections. Small 4-in. diameter holes were punched through the top of the pipe at stations +0, +25, +50, +75, and +100. These holes later provided access for a level rod used to read invert elevations.

Future manhole openings were provided for by scoring the fresh concrete at stations +25, +50, and +75. These manhole rings, punched out successively prior to the use of sections 2, 3, and 4, provided access to each test section for both personnel and strain-gage leads. They also provided later samples of cured-in-place concrete. Figure 2 shows the test layout.

In curing the pipe a polyethelyne film was placed over the fresh concrete. This film was covered in turn with several inches of moist soil. The ends of the pipe were sealed off for the curing period and a few inches of water were introduced into the pipe to provide interior curing moisture.

TABLE 3

PROPERTIES OF GRANULAR BACKFILL MATERIAL

(a) GRADATION

| Sieve Size | Percent Passing |
|---|---|
| 1 1/8 in. | 100 |
| 3/4 in. | 91 |
| 1/2 in. | 77 |
| 3/8 in. | 70 |
| 1/4 in. | 63 |
| No. 4 | 58 |
| No. 10 | 48 |
| No. 20 | 38 |
| No. 40 | 31 |
| No. 80 | 22 |
| No. 200 | 11 |

(b) DENSITIES

Maximum T-99, 134 pcf
Maximum T-180, 143 pcf
Optimum moisture, 5%

Several days before the first load tests were to be run, the pipe was allowed to dry out so that strain gages could be installed. The aggregate base material was also placed during this period. Test Section 1, from station +0 to +25 was covered with 24 in. of compacted backfill in 8-in. lifts. Section 2, station +25 to +50, received 18 in. of backfill; Section 3, station +50 to +75, received 12 in.; and Section 4, stations +75 to 1 + 00, received only 6 in. Results of backfill tests are given in Table 4.

TABLE 4

COMPACTION OF GRANULAR BACKFILL

| Location | Lift | Thickness of Lift (in.) | Moisture Content (%) | Dry Density (pcf) | Percent T-99 Density | Percent T-180 Density |
|---|---|---|---|---|---|---|
| Section 1, | | | | | | |
| 24-in. backfill | Bottom | 8 | 3 | 138 | 103 | 96 |
| | Bottom | 8 | 5 | 141 | 105 | 98 |
| | Second | 8 | 5 | 141 | 105 | 98 |
| | Top | 8 | 5 | 145 | 108 | 101 |
| | Top | 8 | 5 | 138 | 103 | 96 |
| Section 2, | | | | | | |
| 18-in. backfill | Bottom | 6 | 5 | 141 | 105 | 98 |
| | Second | 6 | 5 | 151 | 113 | 105 |
| | Top | 6 | 5 | 141 | 105 | 98 |
| | Top | 6 | 5 | 147 | 110 | 102 |
| Section 3, | | | | | | |
| 12-in. backfill | Bottom | 6 | 6 | 142 | 106 | 99 |
| | Top | 6 | 6 | 145 | 108 | 101 |
| Section 4, | | | | | | |
| 6-in. backfill | Top | 6 | 4 | 143 | 107 | 100 |
| | Top | 6 | 2 | 143 | 107 | 100 |

### Concrete Control

In advance of construction, the proposed mix design and materials were checked for conformance to city specifications. These properties are given in Table 5. During construction, slump and air content were checked frequently with the results. Cylinders and beams were molded from the concrete in each test section and were subjected to standard curing.

## INSTALLATIONS FOR INSTRUMENTATION

### Level Readings

A permanent bench mark was established on the site and a permanent shaded level setup was located. A profile of the trench invert was read prior to construction. Brass plugs were set in the invert of the poured pipe at the ends of the test sections at stations 0, +25, +50, +75, and 1 +00. These plugs were located directly under the 4-in. diameter holes in the top of the pipe (Fig. 2).

### Dial Gages

Dial gages were installed to read changes in horizontal and vertical diameters directly in the plane of one of the wheel loads (Figs. 1 and 2). The gages, mounted on steel bar stock, were typical Ames dials with a least count of 0.0001 in.

### Soil Pressure Cell

A Carlson Type PE-50 pressure cell was used to determine soil pressures under varying conditions (Fig. 1). The pressure cells were located directly in the plane of one of the dual wheels, as were the dial gages. During the first test under 24 in. of cover, the pressure cell was located at the top surface of the pipe with its plane horizontal. For the second and third tests, the cell was located about 18 in. ahead of the vertical axis

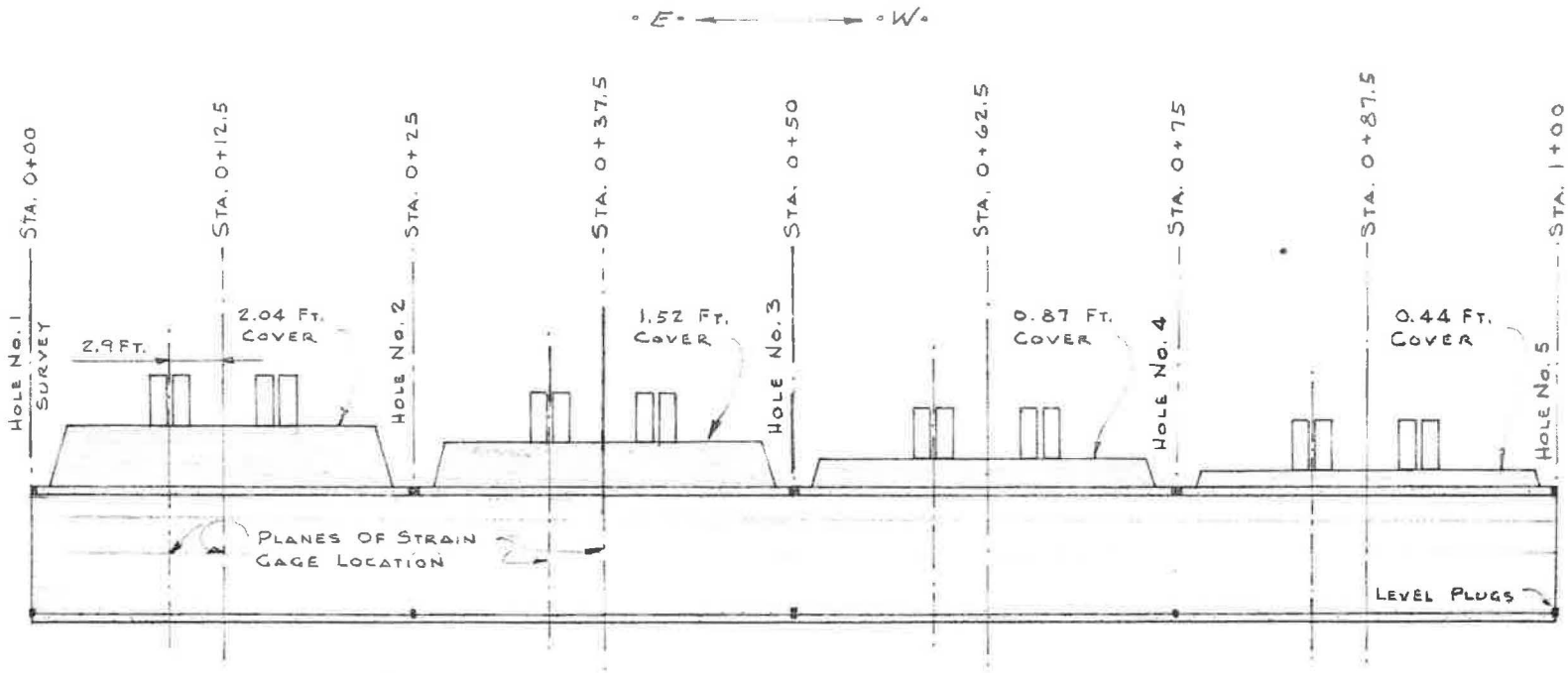


Figure 2. Details of test layout.

TABLE 5

CONCRETE USED IN CAST-IN-PLACE PIPE

(a) MIX DESIGN

| Material | Weight (lb) | Amount |
|---|---|---|
| Cement | 517 | 5.5 sacks |
| Water | 300 | 36 gal |
| Coarse rock | 1,005 | 1,695 lb total coarse agg. |
| Fine rock | 690 | |
| Sand | 1,510 | — |

Additives:
Durair AEA—¾ fl oz per sack
Pozzolith No. 8—¼ lb per sack
Water-cement ratio:
0.580 by weight
6.55 gal per sack

(b) AGGREGATE GRADATION

| Sieve Size | Percent Passing, by Weight | | | |
|---|---|---|---|---|
| | Coarse Rock | Fine Rock | Combined Rock | Sand |
| 1 in. | 100 | — | 100 | — |
| ¾ in. | 90 | 100 | 94 | — |
| ½ in. | 35 | 91 | 58 | — |
| ⅜ in. | 7 | 60 | 29 | 100 |
| No. 4 | 1 | 3 | 2 | 98 |
| No. 8 | 0 | 0 | 0 | 84 |
| No. 16 | — | — | — | 67 |
| No. 30 | — | — | — | 38 |
| No. 50 | — | — | — | 15 |
| No. 100 | — | — | — | 4 |
| No. 200 | — | — | — | 1 |
| Fineness modulus | — | — | — | 3.06 |

(c) TESTS ON FRESH CONCRETE

| Location | Slump (in.) | Air Content (%) |
|---|---|---|
| Sta. 0 + 12.5 | 1¾ | 3.5 |
| Sta. 0 + 37.5 | 1¾ | 3.6 |
| Sta. 0 + 62.5 | 1 | 3.1 |
| Sta. 0 + 87.5 | 2 | 4.6 |

Concrete temperature—90 F

of the pipe with its face on a plane passing through the top of the pipe. For the fourth test, the Carlson pressure cell was located on the outside of the pipe opposite the horizontal diameter and with the plane of the cell vertical.

SR-4 Strain Gages

Strain gages were installed in the interior of the pipe at each test section in two planes. One plane was vertical midway between the wheel loads. The other was vertical

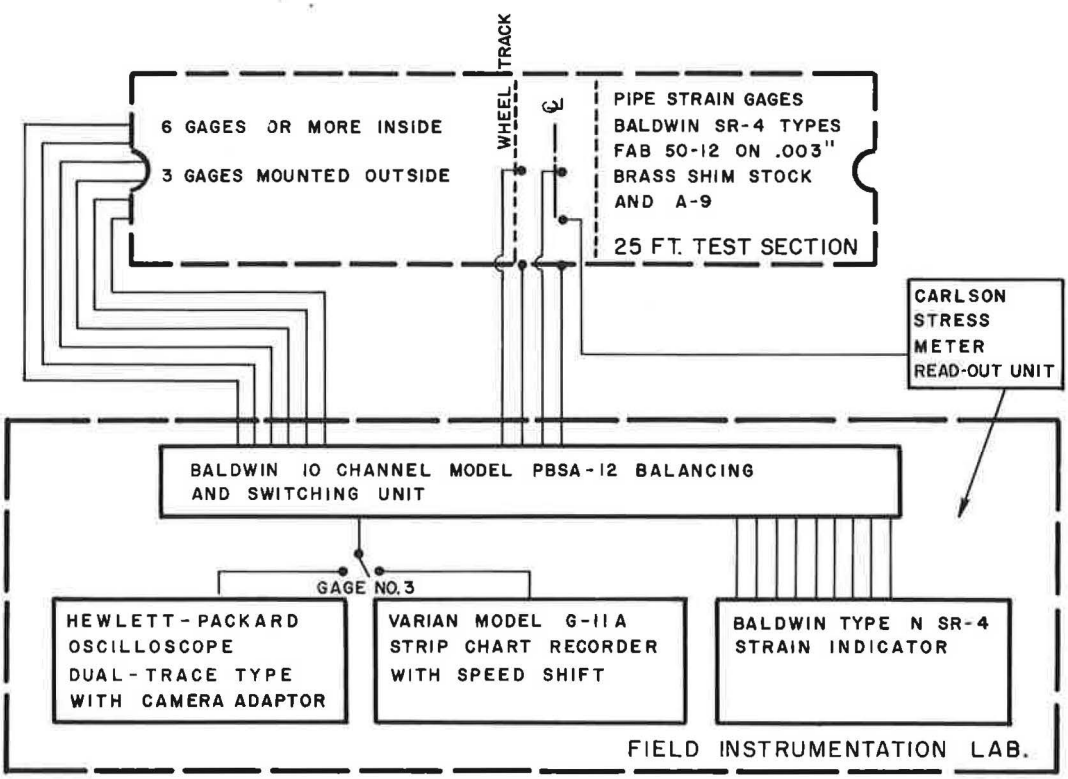


GAGE-TO-GROUND MEASURING EQUIPMENT:

HEWLETT-PACKARD DC VACUUM TUBE VOLTMETER, MODEL 412 A

WATERPROOFING AGENT FOR STRAIN GAGES:

EPOXY-150 AND PETROLASTIC ASPHALT NO. 155 (STANCAL)

STRESS-STRAIN TESTS ON CAST BEAMS AND CYLINDERS, AND PIPE CORES:

300,000-LB., TINIUS OLSON U.T.M. WITH BROWN X-Y RECORDER AND DEFLECTOMETER, MODULUS JACKET, AND SR-4 STRAIN GAGES

CHANGES IN INTERNAL DIAMETER:

BAR-MOUNTED DIAL GAGES, L.L. = .0001 INCH

Figure 3. Strain gage instrumentation.

directly underneath one of the wheel applications. Figure 1 shows the locations of the strain gages within each of the above-described planes. They were located at the top and bottom of the interior of the pipe and at the sides of the pipe, both interior and exterior, at the top of the pipe on the exterior, and at several points above and below the end of the horizontal diameter. All strain gages were placed after the concrete had set, and for only one (exterior at the side) was it necessary to disrupt the natural placement conditions of the pipe.

Each of the four test sections was instrumented with SR-4 Type FAB-50-12 and A-9 resistance wire strain gages. To increase the effective length of the gages, each was bonded to 3-mil brass shim stock strips approximately 6 in. in length. A-9 type gages were attached directly to the concrete surface. EPY-400 cement was used to bond the foil gages to the shim stock, and in turn the shim stock was bonded to the concrete surface with EPY-150 cement. A-9 gages were cemented with standard Duco SR-4 cement. Outside gages, which were exposed to soil and potential mechanical damage, were protected with an asphaltum material over which were applied sponge-resilient pads.

Concrete surfaces receiving the strain gages were prepared with electric stone grinders. Resultant smooth surfaces were thoroughly cleaned with acetone before gage installation. In most instances a minimum of 72 hr elapsed between the time of gage installation and application of test load.

Dummy gages mounted on concrete blocks were placed inside the pipe during the testing program and were used for thermal compensation purposes. To insure that all gages were properly applied, each was visually checked for bond before waterproofing and for gage-to-ground resistance to insure that moisture would not interfere with the test readings. Figure 3 is a schematic layout of the hook-up. All strain gage lead wires, except No. 3, were fed into a switching-balancing unit. Static strain measurements were observed by annual switching into a Baldwin Type N indicator. Gage No. 3, which was located at the top inside under wheel trace position, was fed directly to a strip-chart recorder and oscilloscope.

## TESTING PROCEDURE

### Loading

A flat-bed Ford truck, furnished by the Salt River Project, was used for loading the pipe. This truck was equipped with a single rear axle and dual wheels with 9.00 × 20 tires. The test load was obtained by hoisting oil drums filled with steel balls to the bed of the truck and carefully positioning them so that the load was equally distributed between the two ends of the rear axle. Total axle loads were then measured by the portable scales used by the city for checking truck overloads.

The loads applied on each test section started with 10,000 lb and were increased in 2,000-lb increments to a maximum of 28,000 lb. This maximum was chosen because it is slightly over $1\frac{1}{2}$ times the legal axle load of 18,000 lb in Arizona. Due to lack of distress evidenced in the pipe under the maximum planned loading, Tests II, III, and IV were finished off by loading the bed of the truck with all of the weight available at the site. This amounted to approximately 36,000 lb on the single rear axle.

In each case the truck was driven forward and parked so that the rear axle was above the axis of the pipe. The location was carefully spotted by a transit on an extension of the horizontal axis of the pipe.

### Observations and Readings

All gages were read before the truck moved over the pipe, while the load was centered on the pipe, and again after the truck moved off the pipe. These readings included level shots on the brass plugs in the invert of the pipe at the ends of the test section, observations of the horizontal and vertical dial gages for changes in horizontal and vertical diameters, readings on the SR-4 strain gages in about 13 locations, and the readings on the Carlson pressure cell. In some instances, readings on the Carlson cell were also obtained with the wheel load at different locations on the surface with respect to the vertical line through the pressure cell. Other observations made for each test

were the pressure in the tires and the temperature of the air. Actual tire contact areas under each load were also determined.

## Sequence of Test

Before Loading. —(a) Levels were read on the plugs in the pipe invert at the ends of the test section, (b) unloaded readings were taken on the lengths of the vertical and horizontal diameters, (c) on the SR-4 strain gages, and (d) on the Carlson pressure cell.

Application of Load. —The rear wheels of the truck were placed on the field scale and the bed loaded until the axle load reached the test load (Table 6). The truck was driven forward until the rear axle was directly above the axis of the pipe. The final position was determined by the line of sight of a transit set up on an extension of the pipe axis.

During Load. —After equilibrium in the gages had been reached, the following readings were taken: invert elevations, SR-4 strain gages, horizontal and vertical diameters, and Carlson pressure cell.

After Load. —After the truck had been driven off the pipe, the same readings were repeated for the unloaded condition.

Miscellaneous Readings. —Other determinations made less frequently but at such intervals as necessary to fill out the record included: tire pressures, tire contact areas, and air temperature.

## Concrete Tests

Concrete cylinders cast at the time of the pour were tested periodically to establish a strength-time curve for the concrete used in the pipe. Cylinders were also tested at the same age as each of the test runs. The first test was run at age 28 days, the second at 35, the third at 42, and the fourth at 54 days.

Concrete strengths were also obtained from prisms and cores cut from the pipe and tested at the date of the corresponding test run. These prisms were cut from the concrete manhole covers which were taken out at each test date, carried to the laboratory, and tested. Additional cores were taken from the pipe after the conclusion of the test to establish the extent of the strength-time curve and also to use in additional testing of stress-strain relationships in the concrete. Some of the specimens were tested in simple compression, and some with strain gages attached to the sides. Others were tested to establish the relationship between total stress and total strain in the specimen; the results were recorded on a Brown-Olsen recorder. Laboratory tests with SR-4 observations were also run on load-unload cycles simulating the conditions of the field pipe loading.

To assist in establishing the flexural strength characteristics of the concrete, 6- by 6-in. beams also were cast at the time of pouring the pipe. These beams were tested with SR-4 strain gages attached.

TABLE 6

AXLE LOADS USED IN LOADING[a]

| Nominal Axle Load (lb) | Actual Axle Load (lb) | | | |
|---|---|---|---|---|
| | Test I | Test II | Test III | Test IV |
| 10,000 | 10,000 | 10,030 | 9,940 | 10,000 |
| 12,000 | 12,000 | 12,100 | 11,960 | 12,040 |
| 14,000 | 14,080 | 14,100 | 13,990 | 14,000 |
| 16,000 | 16,030 | 16,070 | 15,930 | 15,940 |
| 18,000 | 17,960 | 18,040 | 18,020 | 17,990 |
| 20,000 | 20,010 | 19,910 | 20,020 | 20,000 |
| 22,000 | 21,930 | 21,910 | 21,930 | 21,950 |
| 24,000 | 24,090 | 24,100 | 23,990 | 23,960 |
| 26,000 | 26,040 | 25,910 | 26,080 | 26,020 |
| 28,000 | 28,050 | 27,900 | 28,050 | 27,930 |
| 36,000 | — | 35,670 | 36,090 | 36,540 |

[a]Truck: 1953 Ford, F-800, 3-ton stake, single rear axle, dual wheels, 16-ft 6-in. wheel base; total weight—8,320 lb; 9:00 x 20 tires, 10-ply, inflated to 70 psi; front axle load varied from 6,230 to 6,590 lb.

## RESULTS

### Level Readings

Level readings on the plugs in the pipe invert indicated a maximum elevation change of 0.02 ft at any point with respect to the original elevation of the points. These data are summarized in Table 7.

Table 8 gives changes in flow line elevation observed during each individual load. Values are given for the two ends of the section being tested. The greatest observed variation from no load to load condition was only 0.008 in.

### Tire Contact Areas and Soil Pressures

Average tire contact pressures are given in Table 9. Table 10 indicates the determinations of soil pressure as measured by the Carlson pressure cell. Test I (24 in. of cover) provides the best record of distribution of soil pressure as the wheel load was directly above the pressure cell. The reduction in intensity was by a factor of 7.2 under 10,000 lb and 4.1 under 28,000 lb. Comparison of pressure readings in Test I, II and III will indicate the rapid reduction in transmitted pressure as the line from the point of application of the load to the pressure cell becomes closer to the horizontal. The low readings of pressure in Test IV show little soil resistance developed at the springline of the pipe under a concentrated load at the center.

Readings of 122 or below are not significant as they are below the sensitivity of the cell. Readings over 7,200 are above the range of the cell and so are likely to be too low.

### Diameters

Table 11 indicates the expected decreases in vertical diameter and increases in horizontal diameter. The changes are small, a maximum of 0.0082 in. or less than 0.02 percent in vertical diameter, and 0.0058 or somewhat over 0.01 percent in horizontal diameter. As found in other measurements involving stress in the concrete, there was some creep evidenced. Figure 4 summarizes this information.

### Concrete Testing

Compressive Tests. — Table 12 lists the compressive strengths obtained on the various types of concrete specimens. These data are shown in a strength-age relationship

TABLE 7

TOTAL VARIATIONS FROM ORIGINAL ELEVATIONS OF FLOW LINE

| | Hole 1 | | Hole 2 | | Hole 3 | | Hole 4 | | Hole 5 |
|---|---|---|---|---|---|---|---|---|---|
| Original elevation | 91.921 | | 91.917 | | 91.995 | | 91.957 | | 91.927 |
| Change from original, ft: | | | | | | | | | |
| Before Test I | 0 | X | 0 | | 0 | | 0 | | 0 |
| After Test I | - 0.003 | | — | | — | | — | | + 0.002 |
| Before Test II | - 0.011 | | + 0.001 | X | + 0.008 | | + 0.012 | | + 0.015 |
| After Test II | - 0.012 | | 0 | | + 0.005 | | + 0.007 | | + 0.013 |
| Before Test III | + 0.019 | | — | | + 0.017 | X | + 0.013 | | + 0.009 |
| After Test III | — | | — | | + 0.020 | | + 0.013 | | + 0.012 |
| Before Test IV | + 0.011 | | + 0.015 | | — | | + 0.013 | X | + 0.007 |
| After Test IV | + 0.010 | | + 0.014 | | — | | + 0.014 | | + 0.008 |

X indicates position of test load.

TABLE 8

VARIATIONS IN ELEVATION OF FLOW LINE (FT)

| Load (lb) | Test I | | Test II | | Test III | | Test IV | |
|---|---|---|---|---|---|---|---|---|
| | Hole 1 | Hole 2 | Hole 2 | Hole 3 | Hole 3 | Hole 4 | Hole 4 | Hole 5 |
| None | 0 | 0 | 0 | 0 | 0 | 0 | 0 | 0 |
| 10,000 | +0.002 | +0.003 | +0.001 | 0 | +0.002 | +0.002 | 0 | -0.001 |
| None | +0.008 | +0.001 | 0 | 0 | +0.003 | 0 | 0 | -0.001 |
| 12,000 | 0 | +0.006 | 0 | +0.001 | +0.001 | 0 | 0 | 0 |
| None | -0.004 | +0.001 | -0.001 | +0.001 | +0.002 | 0 | +0.001 | -0.001 |
| 14,000 | +0.004 | +0.001 | -0.001 | +0.001 | +0.002 | 0 | 0 | 0 |
| None | +0.003 | +0.003 | -0.001 | -0.003 | +0.004 | 0 | 0 | -0.003 |
| 16,000 | -0.001 | +0.001 | -0.003 | 0 | +0.003 | +0.001 | -0.001 | -0.002 |
| None | 0 | +0.005 | 0 | -0.003 | +0.002 | 0 | 0 | -0.002 |
| 18,000 | +0.001 | +0.002 | -0.001 | +0.001 | +0.002 | 0 | 0 | -0.002 |
| None | -0.001 | -0.001 | +0.001 | -0.002 | +0.004 | 0 | -0.001 | -0.001 |
| 20,000 | +0.001 | +0.007 | 0 | 0 | +0.004 | +0.001 | -0.001 | -0.002 |
| None | +0.003 | +0.007 | 0 | -0.001 | +0.004 | +0.002 | -0.001 | -0.001 |
| 22,000 | 0 | +0.004 | -0.001 | 0 | +0.007 | 0 | 0 | -0.002 |
| None | +0.002 | +0.005 | 0 | +0.001 | +0.004 | +0.002 | -0.001 | -0.001 |
| 24,000 | +0.001 | +0.002 | +0.001 | +0.001 | +0.003 | +0.003 | -0.001 | -0.002 |
| None | -0.003 | +0.002 | 0 | +0.001 | +0.004 | +0.002 | 0 | -0.001 |
| 26,000 | 0 | +0.003 | +0.001 | +0.001 | +0.004 | +0.003 | -0.001 | -0.004 |
| None | -0.002 | +0.004 | 0 | 0 | +0.003 | +0.002 | 0 | -0.002 |
| 28,000 | -0.002 | +0.003 | 0 | 0 | +0.004 | +0.001 | -0.002 | -0.001 |
| None | -0.007 | +0.004 | 0 | 0 | +0.003 | +0.002 | +0.001 | -0.002 |
| 36,000 | — | 0 | — | — | +0.003 | -0.002 | — | — |
| None | -0.004 | — | — | — | +0.003 | 0 | — | — |

TABLE 9

TIRE CONTACT AREAS AND PRESSURES

| Nominal Axle Load (lb) | Total Tire Area (sq in.) | Average Contact Pressure (psi) | Average Tire Pressure (psi) | Average Tire Contact Pressure (psf) |
|---|---|---|---|---|
| 10,000 | 107.1 | 46.7 | 71.0 | 6,730 |
| 12,000 | 111.5 | 54.0 | 72.0 | 7,780 |
| 14,000 | 123.3 | 56.7 | 72.0 | 8,180 |
| 16,000 | 133.7 | 59.7 | 72.0 | 8,600 |
| 18,000 | 145.0 | 62.1 | 73.0 | 8,960 |
| 20,000 | 143.9 | 69.5 | 72.0 | 10,000 |
| 22,000 | 151.2 | 72.6 | 72.0 | 10,470 |
| 24,000 | 166.0 | 72.3 | 72.5 | 10,430 |
| 26,000 | 175.1 | 74.4 | 72.0 | 10,710 |
| 28,000 | 185.1 | 76.6 | 73.0 | 11,040 |
| 36,000 | 228.0 | 80.2 | 73.0 | 11,560 |

TABLE 10

DISTRIBUTION OF TIRE PRESSURE TO SOIL PRESSURE GAGE[1] (CARLSON PRESSURE CELL)

| Axle Load (lb) | Gage Pressure (psf) | | | |
|---|---|---|---|---|
| | Test No. I[2] | Test No. II[3] | Test No. III[3] | Test No. IV[4] |
| 0 | 122 | 269 | 122 | 0 |
| 10,000 | 1,053 | 392 | 122 | 73 |
| 12,000 | 1,441 | 392 | 122 | 73 |
| 14,000 | 1,934 | 367 | 122 | 73 |
| 16,000 | 1,763 | 343 | 122 | 98 |
| 18,000 | 2,350 | 416 | 122 | 98 |
| 20,000 | 2,472 | 416 | 122 | 122 |
| 22,000 | 2,374 | 441 | 122 | 122 |
| 22,000 | — | — | 4,968[5] | — |
| 24,000 | 2,791 | 490 | 122 | 122 |
| 26,000 | 2,595 | 490 | 122 | 122 |
| 28,000 | 2,840 | 441 | 122 | 147 |
| 28,000 | — | — | 1,983[5] | — |
| 28,000 | — | — | 2,056[6] | — |
| 28,000 | — | — | 4,651[7] | — |
| 28,000 | — | — | 6,585[8] | 122[8] |
| 36,000 | — | — | 122 | 245 |
| 36,000 | — | — | 7,613[8] | — |

[1] Load over axis of pipe unless otherwise noted.
[2] Cell plate flush with top of pipe at centerline and under west wheel trace.
[3] Cell plate flush with top of pipe but 18 in. north of axis under wheel trace.
[4] Cell plate in vertical plane against soil at spring line of pipe, under wheel trace.
[5] Load 15 in. north of axis of pipe.
[6] Load 15½ in. north of axis of pipe.
[7] Load 16 in. north of axis of pipe.
[8] Load 18 in. north of axis of pipe.

in Figure 5. Values for prisms and cores have been corrected for L/d ratio. A 28-day strength of 4,430 psi is compared to a 35-day strength of 4,600 psi, a 42-day value of 4,770 psi, and 4,940 at 54 days.

Modulus of Rupture Tests. — Three 6- by 6-in. beams were tested at 29 days with an average modulus of 595 psi. Results of these and other beam tests are given in Table 13.

Stress-Strain in Concrete Cores. — Table 14 gives a summary of loading and unloading cycles on cores cut from the pipe. Loading and unloading cycles in 10 increments were applied to the 4-in. cores to simulate the loads applied to the pipe itself. Results of the succeeding compressive tests are also given, as are the calculated values for modulus of elasticity. Figure 6 plots a typical loading-unloading cycle. Figure 7 shows the compression test on the same core. The values for modulus of elasticity as determined by the slope of the stress-strain curve show a decided trend toward a straight-line relationship of decreasing value of E for increasing values of ultimate strength.

## Pipe Strains

Table 15 is an example of the reduced strain readings on the pipe. These data are from Test IV at 54 days with 6 in. of cover. Results obtained on the other three tests were somewhat more erratic due to the low values of the readings. In a general way, readings on the other less severe tests were somewhat inversely proportional to the amount of cover. There are apparent inconsistencies, however.

Corrected results from gage 1, outside top, and gage 3, inside top, are given in Table 16. These are, respectively, the highest strain gage in compression and the highest strain gage in tension. A strain of 393 $\mu$ in./in. compression and 52 $\mu$ in./in. in tension are noted. As is evident throughout, there is appreciable creep in the concrete. Creep determinations were made after 10 min of rebound time. Any further rebound beyond 10 min after unloading was negligible.

## Visual Observations

No observable cracks appeared in the pipe during the loading cycles for any of the four test situations.

Some small circular hairline cracks appeared in the transverse planes through two of the manholes, but these could be attributed to shrinkage at a reduced cross-section. There was no apparent opening of these cracks due to loading.

Two short longitudinal hairline cracks appeared in the bottom of the pipe between stations +50 and +75. These developed between the times of Test II and Test III and had no noticeable change during future loadings.

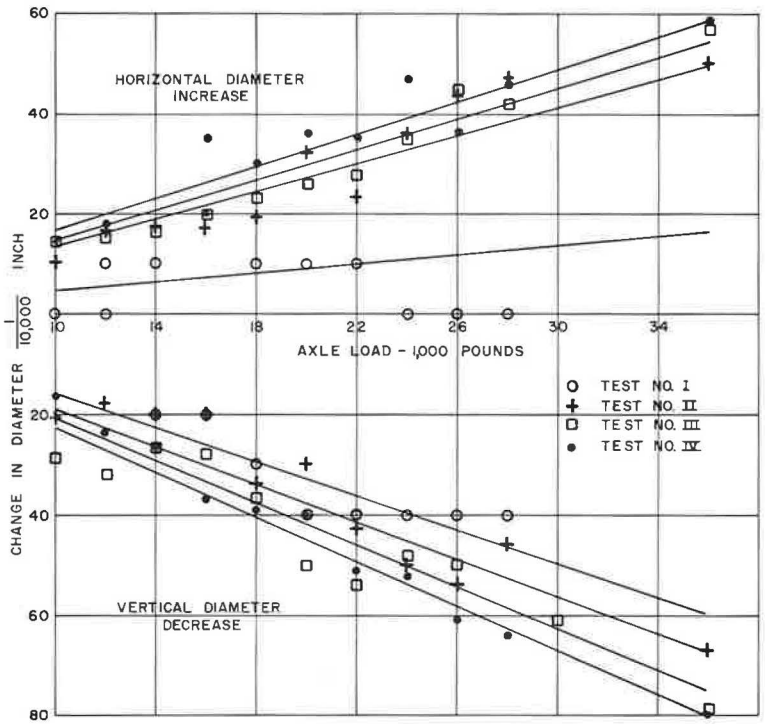


Figure 4. Changes in diameter under load.

TABLE 11

CHANGES IN DIAMETER UNDER LOAD

| Axle Load (lb) | Test I | Test II | Test III | Test IV |
|---|---|---|---|---|
| | (a) VERTICAL DIAMETER (in.) | | | |
| 0 | — | — | — | — |
| 10,000 | 0 | - 0.0021 | - 0.0029 | - 0.0019 |
| 12,000 | 0 | 23 | 32 | 25 |
| 14,000 | - 0.0020 | 20 | 28 | 28 |
| 16,000 | 20 | 20 | 29 | 39 |
| 18,000 | 30 | 31 | 38 | 41 |
| 20,000 | 35 | 31 | 53 | 42 |
| 22,000 | 45 | 42 | 56 | 50 |
| 24,000 | 40 | 50 | 51 | 55 |
| 26,000 | 40 | 56 | 48 | 62 |
| 28,000 | - 0.0040 | 46 | 59 | 67 |
| 36,000 | — | - 0.0067 | - 0.0080 | - 0.0082 |
| Total creep | 0 | - 0.0004 | - 0.0012 | - 0.0032 |
| | (b) HORIZONTAL DIAMETER (in.) | | | |
| 0 | — | — | — | — |
| 10,000 | 0 | 10 | + 0.0014 | + 0.0014 |
| 12,000 | + 0.0005 | + 0.0014 | + 0.0015 | 17 |
| 14,000 | + 0.0010 | 0.0017 | 16 | 18 |
| 16,000 | 15 | 0.0017 | 19 | 24 |
| 18,000 | 25 | 0.0014 | 20 | 27 |
| 20,000 | 20 | 0.0029 | 19 | 34 |
| 22,000 | 20 | 0.0024 | 27 | 35 |
| 24,000 | 5 | 35 | 31 | 43 |
| 26,000 | 0 | 44 | 45 | 34 |
| 28,000 | + 0.0005 | 49 | 45 | 44 |
| 36,000 | — | + 0.0053 | + 0.0056 | + 0.0058 |
| Total creep | + 0.0080 | + 0.0007 | + 0.0023 | + 0.0052 |

TABLE 12

COMPRESSIVE STRENGTHS OF CONCRETE

| Age Days | Location | Compressive Strength (psi) | Type of Specimen |
|---|---|---|---|
| 1¼ | Random | 2,000 | Cylinder by supplier |
| 3 | Random | 2,800 | Cylinder by supplier |
| 3 | Random | 2,820 | Cylinder by supplier |
| 7 | Random | 3,630 | Cylinder by supplier |
| 7 | Random | 3,630 | Cylinder by supplier |
| 14 | Random | 4,000 | Cylinder by supplier |
| 14 | Random | 4,220 | Cylinder by supplier |
| 20 | Random | 4,220 | Cylinder by supplier |
| 28 | Random | 4,550 | Cylinder by supplier |
| 28 | 0 + 12 | 4,240 | Cylinder by laboratory |
| 28 | 0 + 12 | 3,660 | Cylinder by laboratory |
| 28 | 0 + 12 | 4,230 | Cylinder by laboratory |
| 28 | 0 + 12 | 3,750 | Cylinder by laboratory |
| 28 | 0 + 12 | 3,910 | Cylinder by laboratory |
| 35 | 0 + 37 | 4,440 | Cylinder by laboratory |
| 35 | 0 + 37 | 4,790 | Cylinder by laboratory |
| 35 | 0 + 37 | 4,810 | Cylinder by laboratory |
| 40 | 0 + 50 | 3,530 | Prism cut from top of pipe |
| 40 | 0 + 50 | 4,010 | Prism cut from top of pipe |
| 41 | 0 + 50 | 4,470 | Prism cut from top of pipe |
| 41 | 0 + 50 | 3,180 | Prism cut from top of pipe |
| 43 | 0 + 62 | 4,620 | Cylinder by laboratory |
| 43 | 0 + 62 | 4,420 | Cylinder by laboratory |
| 43 | 0 + 62 | 4,420 | Cylinder by laboratory |
| 48 | 0 + 75 | 4,280 | Prism cut from top of pipe |
| 48 | 0 + 75 | 3,840 | Prism cut from top of pipe |
| 48 | 0 + 75 | 4,840 | Prism cut from top of pipe |
| 54 | 0 + 87 | 4,470 | Cylinder by laboratory |
| 54 | 0 + 87 | 4,810 | Cylinder by laboratory |
| 54 | 0 + 87 | 4,490 | Cylinder by laboratory |
| 63 | 0 + 25 | 3,480 | Prism cut from top of pipe |
| 72 | 0 + 12 | 4,360 | Core cut from bottom of pipe |
| 72 | 0 + 37 | 4,860 | Core cut from bottom of pipe |
| 72 | 0 + 62 | 4,960 | Core cut from bottom of pipe |
| 79 | 0 + 12 | 5,590 | Core cut from bottom of pipe |
| 79 | 0 + 37 | 5,240 | Core cut from bottom of pipe |
| 79 | 0 + 87 | 5,460 | Core cut from bottom of pipe |
| 95 | 0 + 12 | 6,270 | Core cut from top of pipe |
| 95 | 0 + 37 | 6,580 | Core cut from top of pipe |
| 95 | 0 + 62 | 6,270 | Core cut from top of pipe |
| 95 | 0 + 87 | 5,470 | Core cut from top of pipe |
| 110 | 0 + 37 | 5,470 | Core cut from bottom of pipe |
| 110 | 0 + 62 | 5,840 | Core cut from bottom of pipe |
| 110 | 0 + 87 | 5,240 | Core cut from bottom of pipe |
| 135 | 0 + 12 | 5,320 | Core cut from bottom of pipe |
| 135 | 0 + 37 | 5,910 | Core cut from bottom of pipe |
| 135 | 0 + 62 | 5,530 | Core cut from bottom of pipe |

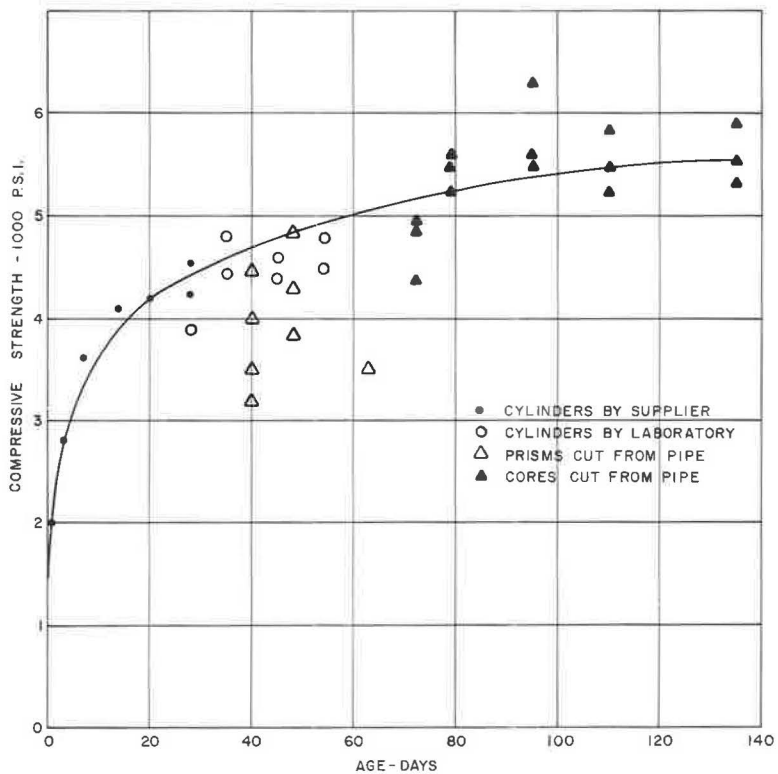


Figure 5. Compressive strengths of concrete.

TABLE 13

RESULTS OF TESTS ON CAST BEAMS

| Location of Beam Section | Age Days | Modulus of Rupture (psi) | Strain at Failure ($\mu$ in./in.) | |
|---|---|---|---|---|
| | | | Tens. | Comp. |
| I | 29 | 500 | 60 | 160 |
| I | 29 | 640 | | |
| I | 29 | 640 | | |
| II | 35 | 500 | 40 | 120 |
| III | 43 | 710 | 120 | 180 |
| IV | 54 | 580 | 115 | 115 |

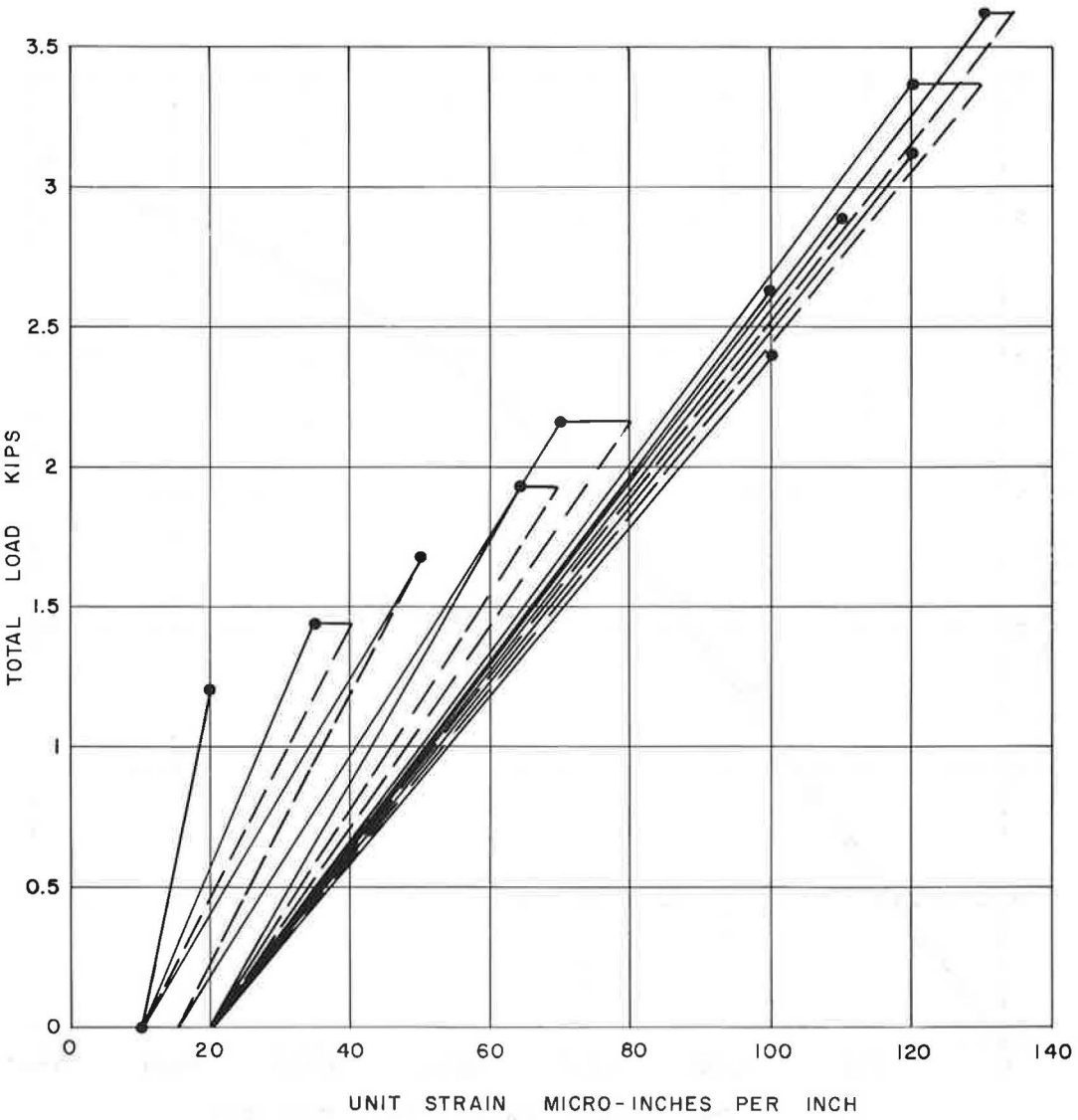


Figure 6. Load-unload cycles, core 3C.

TABLE 14

STRESS AND STRAIN RELATIONS IN CONCRETE CORES

| Core | Location | Age-Days | Load-Unload Cycle | | | | | Stress-Strain Curve | |
|---|---|---|---|---|---|---|---|---|---|
| | | | Initial Load | | Final Load | | Max. Unit Strain | Max. Unit Stress (lb) | Slope of Initial Curve, E (psi × $10^6$) |
| | | | (lb) | Psi | (lb) | Psi | | | |
| 1C | Sta. 0 - 12, top | 95 | 5,000 | 400 | 15,000 | 1,200 | 0.000570 | 6,270 | 3.11 |
| 1D | Sta. 0 + 13, bottom | 135 | 5,000 | 400 | 15,000 | 1,200 | 0.000290 | 5,320 | 4.55 |
| 2C | Sta. 0 + 37, top | 95 | 2,500 | 200 | 7,500 | 600 | 0.000220 | 6,580 | 2.57 |
| 2B | Sta. 0 + 37, bottom | 110 | 2,500 | 200 | 7,500 | 600 | 0.000045 | 5,470 | 6.10 |
| 2D | Sta. 0 + 38, bottom | 135 | 2,500 | 200 | 7,500 | 600 | 0.000315 | 5,910 | 3.80 |
| 3C | Sta. 0 + 62, top | 95 | 1,200 | 100 | 3,600 | 300 | 0.000125 | 6,270 | 3.72 |
| 3B | Sta. 0 + 62, bottom | 110 | 1,200 | 100 | 3,600 | 300 | No test | 5,840 | 4.05 |
| 3D | Sta. 0 + 63, bottom | 135 | 1,200 | 100 | 3,600 | 300 | 0.000060 | 5,530 | 4.03 |
| 4C | Sta. 0 + 87, top | 95 | 15,000 | 1,200 | 45,000 | 3,600 | 0.001550 | 5,470 | 3.96 |
| 4B | Sta. 0 + 87, bottom | 110 | 15,000 | 1,200 | 45,000 | 3,600 | 0.001280 | 5,240 | 4.57 |

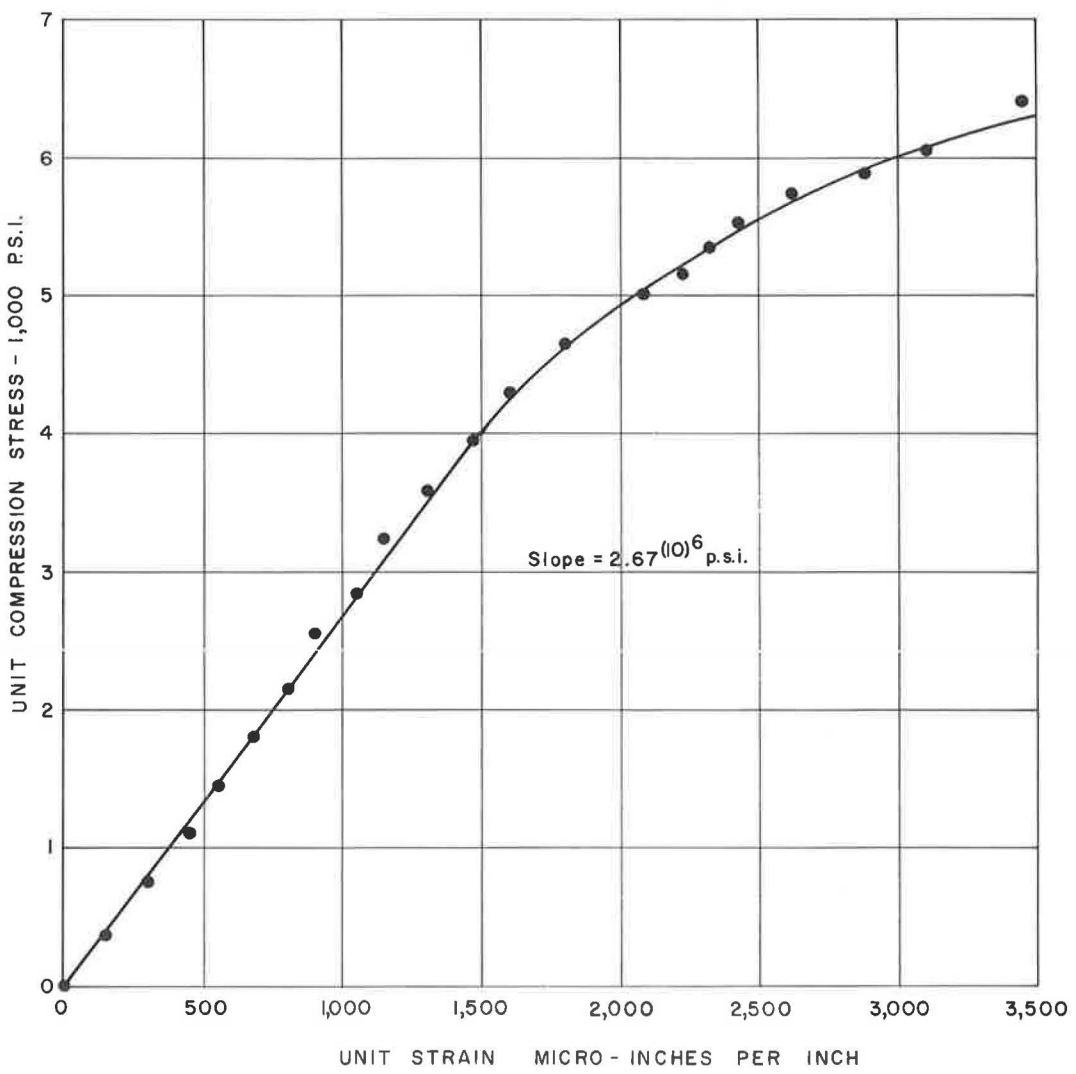


Figure 7. Compression test of core 3C.

TABLE 15

SUMMARY OF STRAIN READINGS—TEST IV[a]

| Load (lb) | Indicated Strain (μ in./in.) per Gage | | | | | | | | | | | | |
|---|---|---|---|---|---|---|---|---|---|---|---|---|---|
| | 1 | 2 | 3 | 4 | 5 | 6 | 7 | 8 | 9 | 10 | 1A | 1B | 3A |
| 10,000 | - 80 | + 5 | +13 | -15 | +10 | - 5 | - 55 | +10 | -20 | + 5 | -20 | - 55 | +30 |
| 12,000 | -100 | 0 | +17 | -10 | +10 | -20 | - 70 | 0 | -35 | +10 | -45 | - 55 | +35 |
| 14,000 | -120 | +10 | +28 | -15 | +10 | -10 | - 35 | +15 | -30 | +10 | -60 | - 75 | +45 |
| 16,000 | -160 | +10 | +23 | -25 | +10 | -15 | - 55 | +20 | -35 | +15 | -50 | - 80 | +50 |
| 18,000 | -160 | +10 | +37 | -25 | +10 | -20 | -100 | +20 | -40 | +10 | -55 | - 55 | +55 |
| 20,000 | -190 | +10 | +53 | -30 | +10 | -25 | - 40 | +15 | -30 | +15 | -70 | - 50 | +60 |
| 22,000 | -125 | 0 | +57 | -35 | +20 | -20 | - 30 | +20 | -50 | +10 | -70 | - 45 | +60 |
| 24,000 | -250 | +20 | +64 | -35 | +25 | -20 | - 65 | +75 | -45 | +20 | -75 | - 80 | +70 |
| 26,000 | -270 | +20 | +72 | -30 | +30 | -20 | -125 | +40 | -40 | +25 | -75 | -100 | +80 |
| 28,000 | -450 | +20 | +71 | -40 | +20 | -25 | -310 | +35 | -55 | +25 | -70 | -145 | +85 |

[a]Plus values indicate tension; minus values indicate compression.

Gage 1 Top-outside, under wheel trace—FAB-50-12.
2 Side-outside, in wheel trace line—FAB-50-12.
3 Top-inside, under wheel trace (Recorded)—FAB-50-12.
4 Side-inside, under wheel trace—FAB-50-12.
5 Bottom-inside, under wheel trace—FAB-50-12.
6 Top-outside between wheel traces, at midpoint—FAB-50-12.
7 Side-outside, midpoint between wheels—FAB-50-12.
8 Top-inside, midpoint between wheels—FAB-50-12.
9 Side-inside, midpoint between wheels—FAB-50-12.
10 Bottom-inside, midpoint between wheels—FAB-50-12.
1A Outside-top, 6 in. west of no. 1 gage @ ℄ —FAB-50-12.
1B Outside-top, 12 in. west of no. 1 gage @ ℄ —FAB-50-12.
3A Inside-top, 12 in. west of no. 3 gage @ ℄ —A-9.

TABLE 16

TYPICAL STRAIN GAGE RESULTS—TEST NO. 4

| Axle Load (lb) | Gage at Outside Top of Pipe | | Gage at Inside Top of Pipe | |
|---|---|---|---|---|
| | Elastic Strain per Load (μ in./in.) | Creep Strain per Load (μ in./in.) | Elastic Strain per Load (μ in./in.) | Creep Strain per Load (μ in./in.) |
| 0 | 0 | 0 | 0 | 0 |
| 10,000 | - 34 | -34 | + 7 | + 4 |
| 12,000 | - 42 | -43 | +15 | 0 |
| 14,000 | - 42 | -60 | +22 | + 2 |
| 16,000 | - 85 | -91 | +20 | 0 |
| 18,000 | -111 | -25 | +30 | + 2 |
| 20,000 | -111 | -51 | +36 | + 9 |
| 22,000 | -100 | 0 | +38 | +11 |
| 24,000 | -195 | -17 | +44 | +11 |
| 26,000 | -247 | +17 | +54 | + 7 |
| 28,000 | -393 | -77 | +52 | + 9 |

Following the final test, a 2,740-lb "skull-cracker" was dropped from a height of 34 ft onto the pipe with 6 in. of cover. A rough circular hole was opened up about 18 in. in diameter (the approximate diameter of the ball). The weight did not enter beyond the inner surface of the pipe. One small circumferential crack was opened up leading away from the hole. No other cracks were observed.

## ANALYSIS OF RESULTS

### Installation

The test section may be assumed to be a standard good installation, typical of the process. The concrete was a normal material for the area and the soil conditions were not untypical. The backfill was compacted to a slightly greater density than typical for such a construction.

### Invert Elevations

Variations in elevation of the invert were not great and show no particular pattern. It can be assumed that the soil provided adequate bedding for the loads applied and that there was no significant settlement and no cracking due to settlement of the pipe.

### Tire and Soil Pressures

There are several significant facts indicated in the results of the readings on the Carlson pressure cell:

1. Readings from Test I indicate that the greater the area of surface application of load and the greater the intensity, the greater the percentage of load which reaches a certain plane beneath it.
2. Readings in Test III strongly illustrate the importance of lateral position of the load with respect to the pressure cell on the amount of pressure recorded by that cell. Because of this importance, slight errors in positioning of load noticeably reduce the consistency of the data.
3. The small values observed in Test IV with maximum load in the pipe and with minimum cover indicate the rigidity of the pipe. Within the range of loading, there is apparently little passive soil resistance mobilized.

### Diameters

Two specific observations may be made with respect to the changes in diameter under load:

1. The diameter changes under load are too small to cause concern within the load range tested.
2. Creep of the concrete is evident even under the lighter load situations.

This permanent increase in horizontal diameter will help the pipe to maintain contact with the adjacent soil and so gain what support it can use in that direction.

### Concrete Tests

The usual variations in concrete test results were again observed here. The practice of combining cylinders and cores in a single curve may be questioned, but it has no strong effect on the interpretation of results. The rather low values of strain at failure in the beams, particularly on the compression side, are difficult to correlate.

The loading and unloading cycles on the cores produced two features worthy of emphasis:

1. The creep was again strongly evident even under light loads.
2. Whereas the fresh concrete specimen will probably have a stress-strain curve which has no tangent section, such a curve when resulting from a test on a previously loaded and unloaded specimen will have a tangent section for about two-thirds of its range (Fig. 7).

Because the usual pipe installation will be subjected to continuous and repeated loadings, it is reasonable to expect that the stress-strain curve may be a straight line. There is further indication that the slope of this line (the modulus of elasticity) is flatter (smaller) for stronger concrete.

### Pipe Strains

Indications are that, with lighter loads, the accuracy of the SR-4 strain gages on a heterogeneous material such as concrete is not such as to produce consistent or significant results. Observations need to be made accurately and analyzed with care to separate creep from elastic strain.

## CONCLUSIONS

A modulus of elasticity of 4,000,000 psi, an ultimate compressive strength of 4,000 psi and a safe fatigue limit of 50 percent of the ultimate, yields a design stress of 2,000 psi and a safe strain in compression of 500 $\mu$ in./in. This strain was not exceeded under the 28,000-lb load, even with only 6 in. of cover. A tensile stress (and hence strain) equal to one-tenth the value in compression, yields a safe strain in tension of 50 $\mu$ in./in. However, modulus of rupture is about one-seventh of the compressive strength, so that a strain of $\frac{1}{7} \times 500$ or 71 $\mu$ in./in. is obtained for the tension fibres in flexure. This figure was met in the test and exceeded only slightly.

Therefore, it may be assumed that the installation tested with only 6 in. of cover could carry an unlimited number of static axle loads which exceed the legal limit by 50 percent. If the depth is doubled to allow for an undetermined increase in load because of impact, a minimum safe cover of 12 in. is needed for this type of installation.

Little is really known of the action and stress distribution in a structure such as this. Much more research of this type is needed so that a rational basis may be reached for design of such pipes.

The common SR-4 strain gage appears definitely limited in its application to work of this type. The newly-developed semi-conductor strain gages promise to be much more useful in the concrete structures instrumentation field. These gages have an output about 50 times greater than the conventional strain gages used for this test and can be matched to a thermal differential of six parts per million. This type of gage will be much more satisfactory for low-level strains in both static and dynamic studies. Micro triaxial strain devices are also being developed for embedment in the concrete.

Studies should be made concerning the effect of vehicle impact on underground pipes as related to depth and type of cover. The commonly used factors may be too large for this type of installation—even with only 6 in. of cushioning backfill. Semiconductor gages and oscillographic records should give excellent records.

## ACKNOWLEDGMENTS

Gratitude is expressed to the following personnel of the City of Phoenix: Clint Warren, Lloyd Anderson, Sid Favour, A. Morgan Johnson, Gerry Maughan, Sam Tucker, and Fred Glendening. Thanks are due to Henry Shipley of the Salt River Project and Phil Congrove of Southwest No-Joint.

## REFERENCES

1. Abernethy, L. L., "Effect of Trench Conditions and Arch Encasement on Load-Bearing Capacity of Vitrified Clay Pipe." Ohio State Univ. Eng. Exp. Sta., Bull. 158 (Nov. 1955).
2. Eff, K. S., and Ahlvin, R. G., "Very Heavy Aircraft Loads on Pipe Installed Beneath Rigid Pavement." HRB Proc., 40: 475-487 (1961).
3. Clarke, N. W. B., and Young, O. C., "Loads on Underground Pipes Caused by Vehicle Wheels." Proc., The Institution of Civil Engineers, 21: 91-114 (Jan. 1962).
4. Fortier, E. C., "Load Test on 60-Inch No-Joint Concrete Pipe." No-Joint Concrete Pipe Co. (1957).

5. Heger, F. J., "The Strength of Pre-cast Concrete Pipe Reinforced with Welded Wire Fabric." American Iron and Steel Institute (1961).
6. Keeton, J. R., "Strain Distribution in Compressively-Loaded Concrete Specimens." U. S. Navy Civil Eng. Lab. Report (1962).
7. Shipley, H., "Cast-in-Place Pipe for Irrigation." Western Construction (Nov. 1957).
8. Weissmann, G. F., "Strength Requirements for Round Conduit." The Bell System Tech. Jour., No. 3, 737-755 (1957).
9. Weissmann, G. F., and Mitchel, D. M., "Effects of Tamping and Pavement Breaking on Round Conduit." The Bell System Tech. Jour., No. 6, pp. 1551-1581 (1959).
10. Womack, D. E., and Kirdar, E., "Loads and Minimum Cover for Cast-in-Place Unreinforced Concrete Pipe." Salt River Project (1960).

# Formulas to Determine Stone Size for Highway Embankment Protection

ROBERT M. CARMANY, Assistant Design Engineer, California Division of Highways

•A SHOALING water formula to calculate stone size is derived by first, introducing a new concept of the effect of face slope, second, relating forces to potential breaker height, and third, relating breaker height to depth of water. Wave forecasting thus becomes unnecessary under most conditions.

The shoaling water formula is then modified for application to stream-bank and deep-water shore protection.

## SHOAL WATER WAVES

Let line CP (Fig. 1) be drawn between the center of gravity of an outer stone and its point of contact with the stone below. If all stones were perfect spheres and perfectly arranged, the line CP would be parallel to the face slope $\alpha$. But with irregularly shaped stones the direction of CP will vary and CP for the most precariously situated stone will make the greatest angle with the face slope $\alpha$.

Experiments were made with small stones arranged as riprap in which all but the outer stones were held rigidly in plaster of Paris. The face angle was tilted upward until the first uncemented stone fell out (Fig. 2). Repetitions of this experiment indicated that if the stones are fairly well placed, the face slope will reach an angle of 65 or 70 degrees before the line CP of the least stable stone reaches the vertical and the stone falls out (Fig. 3).

Let $\rho$ represent this maximum angle of $\alpha$. Then all angles of $\alpha$ less than $\rho$ will be in a more stable condition as regards wave action, although the stability at angles greater than the angle of repose will be insufficient to resist the forces of gravity. The angle $\rho$ may be compared to the angle of shear within a granular material such as sand. The angle of repose does not represent the angle of shear within the material prior to resting at the angle of repose. The interior angle of shear will be found to be closer to twice the angle

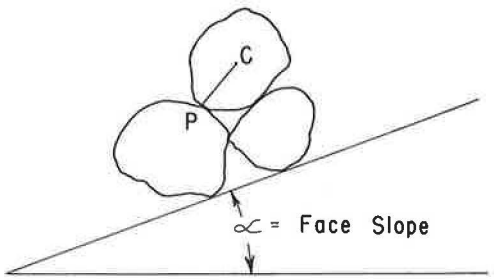


Figure 1. Typical outer stone.

Figure 2. Outer stones stable at $\alpha = 70° +$.

Paper sponsored by Committee on Surface Drainage of Highways.

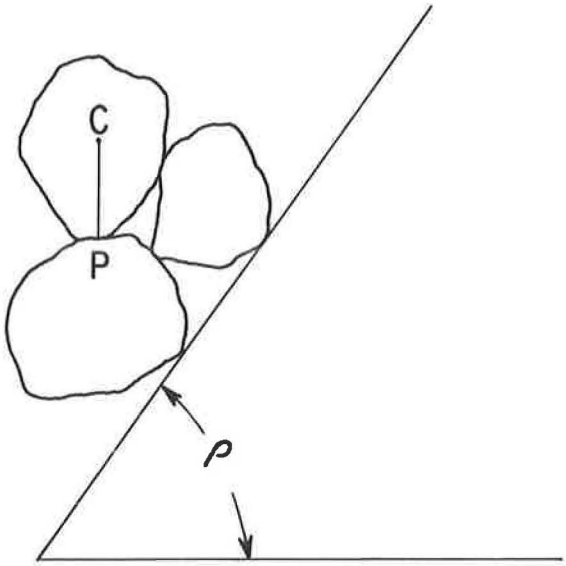


Figure 3. Typical outer stone at equilibrium.

of repose, and riprap, although not sufficiently stable to stand unaided steeper than the angle of repose, does increase in resistance to wave action starting from an angle much steeper.

In the case of the perfectly arranged uniform spheres, resistance to instability would increase starting at $\rho = 90^0$. For irregularly shaped stones, $\rho$ will be in the neighborhood of 65 or 70 degrees. A lesser value has not been used to introduce a factor of safety. The actual experimental value has been used which in turn should reflect the proper relation between the face angle of the riprap and the size of stone. A factor or factors of safety may be introduced later into the final formula.

The minimum force that will dislodge the stone will be that required to rotate the stone about its point of contact P (Fig. 1). The vector diagram for this condition is shown in Figure 4.

Because the force to dislodge the stone will be supplied by the water, $W_S$ will be the submerged weight of the stone and may be expressed:

$$W_S = k_1 d^3 (den_r - den_w) \quad (1)$$

in which

$d$ = a linear dimension of the stone;
$den_r$ = density of the rock;
$den_w$ = density of the water; and
$K_1$ = a constant such that $k_1 d^3$ equals the volume of the stone.

The minimum force necessary to dislodge the stone will be

$$F_1 = k_1 d^3 (den_r - den_w) \sin(\rho-\alpha) \quad (2)$$

The farther the face slope of the riprap is laid back, the more force and energy will be required to dislodge the stone. The required energy could be supplied by the water without the necessary force, but it is hardly likely that the necessary force to move the stone would be of such short duration that the energy was insufficient to displace it. Therefore, assume that for stability the stone must be of sufficient weight to resist the maximum force exerted by the water. The resistance of a body to high-velocity fluid flow is approximately proportional to the square of a lineal dimension of the body, the square of the velocity of the

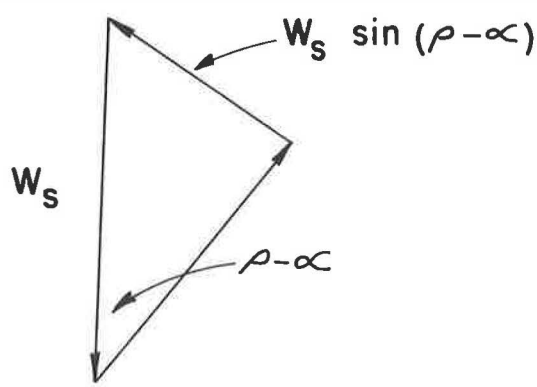


Figure 4. Vector diagram for an outer stone at equilibrium.

fluid past the body, and the density. Therefore, the force exerted by the water on a stone may be expressed as

$$F_2 = k_2 d^2 v^2 den_w \tag{3}$$

Along streams the velocity will not be the average stream velocity, but will vary with location. Along tangents it will be the bank velocity, but at bends it will be the impinging velocity which may approach the thread velocity.

Along larger rivers, lakes and oceans, it will be the maximum velocity resulting from wave action.

Energy contained in deep-water swells is approximately proportional to the length of the wave and the square of the height (1). In general, the more energy involved, the greater will be the damage potential. But this is not the whole story for one can easily visualize that a low wave of extremely long length could have a large amount of energy but exert very little force in deep water. In shoaling water energy concentrates; it depends on the ratio of wave height to wave length, wave period, conditions of shoaling and other things as to how the energy will be concentrated and how much of this energy will be finally dissipated against the riprap. A rather simple way of summarizing the resultant of all these factors on the damage potential at the riprap is to measure the maximum height to which this available energy and any additional that is added by backwash will lift a breaking wave at the riprap. The height of the breaking wave will enable calculation of the maximum velocity of the water impinging on the riprap by the simple relation:

$$v^2 = k_3 H_b \tag{4}$$

in which

$v$ = velocity of the water at the trough, and
$H_b$ = breaker height crest to trough.

Eq. 4 neglects the forward velocity of the breaking wave which should be small compared to the downward velocity at the trough. At higher elevations in the riprap the forward velocity would become more important but still the resultant velocity would be less.

For critical equilibrium $F_1$ must equal $F_2$, hence

$$K_1 d^3 (den_r - den_w) \sin(\rho-\alpha) = k_2 d^2 v^2 den_w \tag{5}$$

The weight of the stone in air may be expressed:

$$W = k_4 d^3 den_r$$

or

$$d^3 = \frac{W}{k_4 den_r} \tag{6}$$

Substituting Eqs. 4 and 6 into 5 and combining all constants results in the following for the required weight of stone:

$$W = \frac{k_5 H_b^3 den_w^3 den_r}{(den_r - den_w)^3 \sin^3(\rho-\alpha)} \tag{7}$$

Most of California's highway embankments along the shore, especially the ocean shore, are not in deep water and some are not even wet except at high tide, so usually waves generated in deep water will be shoaling as they approach the embankment. Under these circumstances there will be a maximum size wave that will reach it still in possession of most of its deep-water energy. This maximum size wave which will expend its energy upon the embankment would ordinarily break at this depth of water. Larger deep-water waves will break in deeper water and will have spent a large portion

of this energy before reaching the embankment. Waves that would ordinarily break in shallower water will, of course, reach the embankment but will contain less energy. Thus, the wave that would ordinarily break at the depth of water near the embankment will expend a maximum amount of energy upon the protection.

The height of this breaking wave, which is the criterion of damage potential adopted in Eq. 7, bears a relation to the depth of water.

For various beach slopes and wave shapes, Figure 5 (2) shows the relation between the height of breaker and the depth of water at which the wave will break when shoaling.

These data are the results of wave tank experiments. They show that for a steep beach slope (1:10), waves with a height to length ratio of approximately $H_o/L_o = 0.02$) ($H_o/T^2 = 0.1$) will produce the highest breakers for any given depth. Their height can be as much as 1.25 times this depth of water $d_b$ (flatter slopes give lower breaker heights). Thus, considering all factors most unfavorable except depth of water which is known, $d_b$ may be substituted for $H_b$ in Eq. 7 and absorb the value of 1.25 in the constant.

$$W = \frac{K_s\, d_b^3\, den_w^3\, den_r}{(den_r - den_w)^3 \sin^3(\rho-\alpha)} \tag{8}$$

All experimental work relating stone size to breaker height has been done on a small scale with artificial waves less than 10 in. high. Considerable trouble can result from extrapolating into the unknown from an empirical or partially empirical formula derived from small-scale experiments. However, once the form is determined from small-scale tests, it may be fitted to full-scale experience by means of the constant. Fortunately for construction, but unfortunately from the standpoint of furnishing data to develop an equation, very few failures resulted that could be directly attributed to wave action. On the Ventura County coast, 3-ton stones resting on a 1.5 to 1 slope were displaced during a severe storm. The depth of water at this time was approximately 7 ft. Damage was minor (Fig. 6). Waves in this area at other times have been estimated to be 7 ft high but did no damage.

On this same coast in an area of greater exposure, 12-ton stones successfully resisted waves estimated to be 12 ft. With no experience with designs failing as a result of insufficient stone size, the constant $K_s$ has been set at 0.003 to agree with minimum stone sizes which proved adequate. As data build up, it is quite possible that this constant may be reduced.

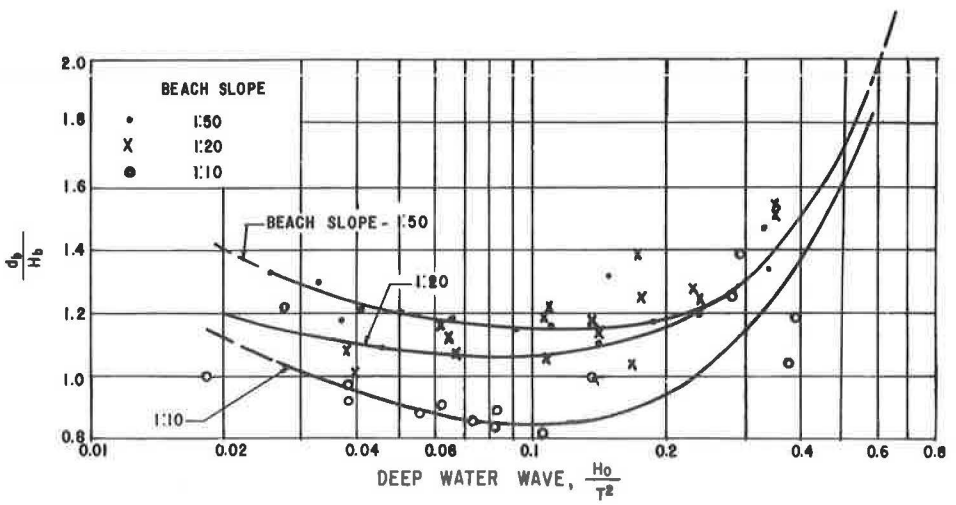


Figure 5. Breaker depth index (2).

Figure 6. Displaced stones after severe storms.

## STREAM FLOW

Whether it be by wave action or stream flow, it is the velocity of water against the riprap that displaces the stones. As stated previously, it seems reasonable that the breaking wave concentrates and transforms the energy into high velocity flow, and neglecting forward velocity, the relation between the height of breaker and velocity of water against the riprap is

$$H_b = \frac{v^2}{2g} = \frac{v^2}{64.4} \tag{9}$$

From Iversen's data (Fig. 5), the maximum height of breaker in relation to depth would be $H_b = 1.25\ d_b$. Therefore, $d_b = v^2/80$.

Substituting $v^2/80$ for $d_b$ in the shallow water formula gives:

$$W = \frac{0.003 \frac{v^6}{80^3} den_w^3\ den_r}{(den_r - den_w)^3 \sin^3(\rho-\alpha)} = \frac{1.17 \times 10^{-5} v^6\ den_w^3\ den_r}{(den_r - den_w)^3 \sin^3(\rho-\alpha)} \tag{10}$$

The constant of 1.17 has been increased to 2. The values obtained then agree with a table that had been in general use in California and which was based on experience of the Division of Highways Joint Bank Protection Committee.

It may be noted that this increase in the constant is the equivalent of an increase in stream velocity of less than 10 percent.

## DEEP-WATER WAVES

The California Division of Highways experience with deep-water protection is very limited. By substituting significant wave height $H_{1/3}$ for $H_b$ and using a constant of $231 \times 10^{-5}$, Eq. 7 then agrees with Iribarren's formula for a slope of 1¾-1 and with the Army Engineers' method (1) for all slopes between 1¼-1 and 3-1 providing the Army K is always taken for the most severe wave shape. Its relation to the formulas of other investigators is shown in Figure 7.

The formulas in slightly altered form used by the California Division of Highways (3) are as follows:

Shoal water:

$$W = \frac{0.003 d_b^3\ sg_r \csc^3(\rho-\alpha)}{\left(\frac{sg_r}{sg_w} - 1\right)^3} \tag{11}$$

Stream flow:

$$W = \frac{0.00002\ v^2\ sg_r \csc^3(\rho-\alpha)}{(sg_r - 1)^3} \tag{12}$$

Deep water:

$$W = \frac{0.00231\ H_{1/3}^3\ sg_r \csc^3(\rho-\alpha)}{\left(\frac{sg_r}{sg_w} - 1\right)^3} \tag{13}$$

$\rho = 70^0$ for broken rock.

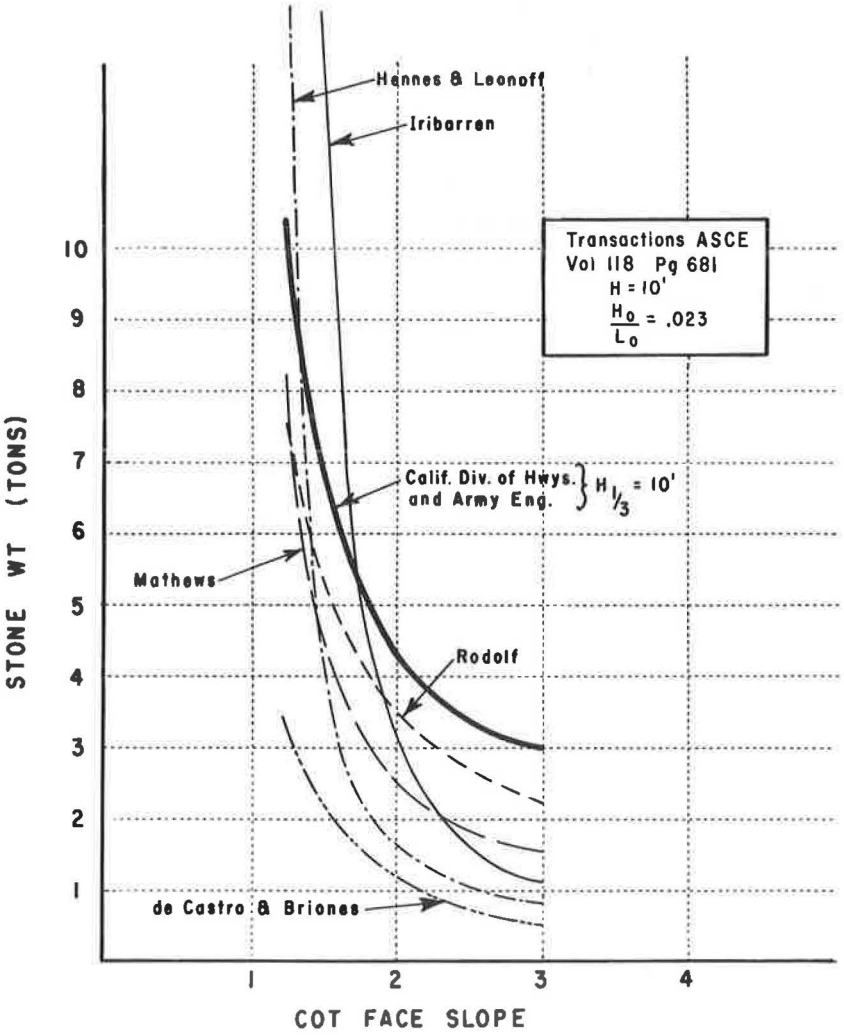


Figure 7. Comparison of formulas (4).

## REFERENCES

1. "Coastal Engineering." p. 10 (Oct. 1950). Also, "Tech. Rpt. #4, Beach Erosion Bd., Corps of Engineers.
2. Iversen, H. W., "Waves and Breakers in Shoaling Water." Proc., Third Conf. on Coastal Engineering.
3. "Bank and Shore Protection in California Highway Practice." (Nov. 1960).

# Riprap Requirements for Overflow Embankments

THOMAS E. MURPHY and JOHN L. GRACE, JR., U. S. Army Engineer Waterways Experiment Station

•OVERFLOW embankments will be integral parts of navigation dams presently being designed and constructed on the Arkansas River. These embankments will be provided across low overbank areas and chutes where necessary to maintain the normal upper pools. In some cases, to provide access to the lock, the embankments will support roadways.

A typical dam will consist of a gated spillway and navigation lock within the main channel of the river and flanking embankments on the overbank. The structures are designed to provide adequate depths for navigation during low flow periods and to offer minimum resistance to flood flows. The capacity of the gated spillways will be such that it will be possible to maintain normal pools until tailwater levels are within about 3 ft of the pool elevation. Thus, when pools rise above normal elevations and overtop the embankments, the differential between headwater and tailwater will not exceed about 3 ft and in most cases will be less than 2 ft.

There will be a total of about 7 miles of these overflow embankments in dams 2-9 and at least some of the embankments can be expected to be overtopped yearly. With this frequency of use, design engineers considered that the embankment sections should be so constructed that extensive repair or maintenance would not be required following each overflow. Several methods of protecting these embankments against scour, including use of asphalt, soil cement, articulated concrete mat, grouted riprap, and dumped stone, were considered. An adequate thickness of protection stone with sizes established on the basis of expected wave heights and velocity of overflow on both the upstream and downstream slopes of the embankments was judged to offer the most satisfactory and economical overflow protection.

Fill slopes for the embankments are being designed in accordance with soils mechanics principles based on the shear strengths of the fill and foundation soils. However, consideration is being given to use of a relatively flat downstream slope to support safely protection stone of the required size and gradation to resist the attack of flowing water. Slopes of 1 on 3 for the upstream face and 1 on 4 for the downstream face are believed to be about optimum from a consideration of all factors.

Thus, it became the purpose of the series of model tests to determine riprap requirements for typical overflow embankments (in Fig. 1). The embankment without a roadway was 6.75 ft high, had a 1 on 3 upstream face, a 24.5-ft wide crown, and a 1 on 4 downstream face. The particular gradation of riprap used on each face was continued to the center line of the crown. The access type embankment studied in the model was 10 ft high, had a 1 on 3 upstream face, a 32.5-ft crown width of which 22 ft was paved roadway, and a 1 on 4 downstream face. The particular gradation of riprap used on each face was continued to the edge of the roadway.

Tests were conducted in a 1:4 scale model (Fig. 2) which reproduced a 40-ft wide section and included 90 ft of approach channel, the overflow embankment and 140 ft of exit channel. The model embankments were molded in sand to the desired shape over a brick cutoff wall which prevented seepage through the embankment. A fiber glass cloth was placed over the sand to serve as a filter and prevent migration of the sand through the voids of the stone. Gravel or crushed rock filters are planned for use in the prototype. However, it is felt that the fiber glass cloth adequately performed the function of these filters in the model and at the same time made re-sorting of the riprap and restoration of damaged portions of the embankment much easier than would have been possible with a coarse sand or gravel filter.

Paper sponsored by Committee on Surface Drainage of Highways.

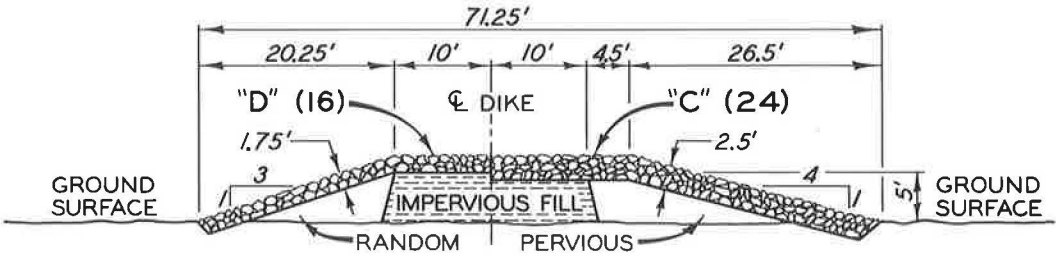


NON-ACCESS TYPE EMBANKMENT

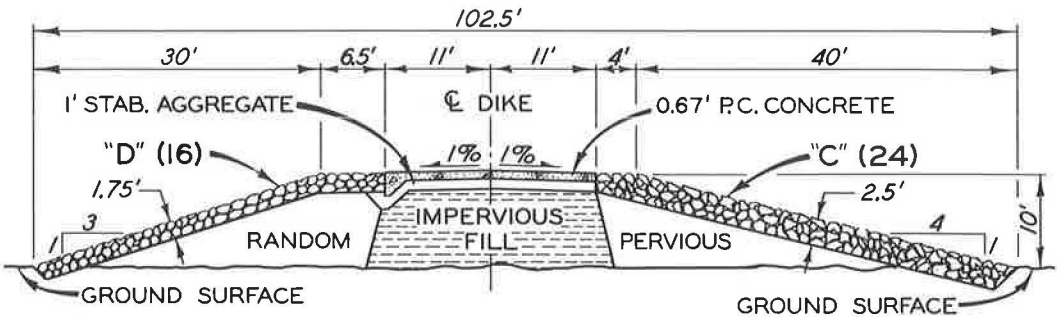


ACCESS TYPE EMBANKMENT

Figure 1. Embankment sections.


Figure 2. General view of model.

Water used in operation of the model was supplied by a pumping system with a capacity of 100 cfs. Discharges entering the model were measured by a calibrated Cole pitometer installed in a 36-in. pipe. Water-surface elevations were measured by point gages supported on steel rails set to grade along the sides of the flume. Tailwater elevations were regulated by a flap gate at the end of the flume.

The accepted equations of hydraulic similitude, based on gravity as the dominant force, were used to express mathematical relations between dimensions and hydraulic quantities of the model and prototype. Scale relations, model to prototype, were as follows:

| Dimension | Ratio | Numerical |
|---|---|---|
| Length | $L_r$ | 1:4 |
| Area | $A_r = L_r^2$ | 1:16 |
| Weight | $W_r = L_r^3$ | 1:64 |
| Velocity | $V_r = L_r^{1/2}$ | 1:2 |
| Discharge | $Q_r = L^{5/2}$ | 1:32 |

The stone used in the model tests was obtained from one of the quarries in the project area and was considered representative in unit weight and shape of pieces of that which will be used in the prototype. It was a nepheline syenite with a specific gravity of 2.63 (164 pcf). The stone was shipped from the quarry in the approximate sizes required but some crushing and final grading of the riprap was accomplished at the Waterways Experiment Station (Fig. 3). Gradation was accomplished by the use of sieves to obtain the desired mean diameters. Average particle weight was then determined from representative samples of each size. It was found that the average weight of each stone approximated the weight of a spherical stone of the diameter considered.

The test section was constructed in the dry (Fig. 4) and then the model was flooded by introduction of water on each side of the test section. With a high tailwater, the desired discharge through the model was established. Tailwater depth was decreased slowly until movement of the stone was observed. This flow condition was allowed for 30 minutes and then a water-surface profile was obtained, the flow was stopped, the model drained slowly and a profile of the disturbed portion of the riprap was made. Flow conditions which resulted in failure at discharges of 20 and 60 cfs are shown in Figures 5 and 6. In the tests, failure of the stone was defined as that condition where all sizes of stone were moved over a considerable area. This did not require that the depth of scour be equal to or greater than the depth of the riprap blanket. The test section following movement of the riprap by a discharge of 60 cfs is shown in Figure 7.

Riprap and water-surface profiles before and after failure for each of the two types of embankments are shown in Figure 8. All failures occurred at the top of the downstream slope. Indications are that failure was caused by a combination of velocity and uplift pressure. The uplift pressure resulted from percolation of flow up the downstream face of the embankment to the vicinity of the crown. Also in all cases the disturbed stone formed a "lip" (Fig. 8) and deflected flow along the surface of the tailwater. Under no conditions was there movement of the type D stone (maximum 200 lb) on the upstream faces of the embankments.

Figure 9 shows the headwater-tailwater conditions under which failure of the access type embankment occurred. Gradations A and $A_1$, and gradations B and C failed under the same conditions. This also was true in the non-access type embankment (Fig. 10). The gradation curves (Fig. 3) show that although gradation A had maximum pieces 36 in. in diameter (2,300 lb) as opposed to 24 in. (700 lb) for gradation $A_1$, stones 16 in. in diameter (200 lb) constituted 50 percent of each of these gradations. Also gradation C had maximum pieces 24 in. in diameter as opposed to 16 in. in gradation B, but 75 percent of each of these gradations consisted of stone 10 in. in diameter (50 lb) or smaller. In the model tests, the large pieces in gradations A and C were dislodged by undercutting resulting from removal of the smaller pieces. Thus it appears that the critical size stone in each gradation is that stone which represents a certain percentage of the total. For the case at hand it seems that the critical size stone is that which represents 60 to 65 percent of the total. In other words, the pieces of stone which are larger than those which represent 60 to 65 percent of the total do not increase the effectiveness of the particular gradation.

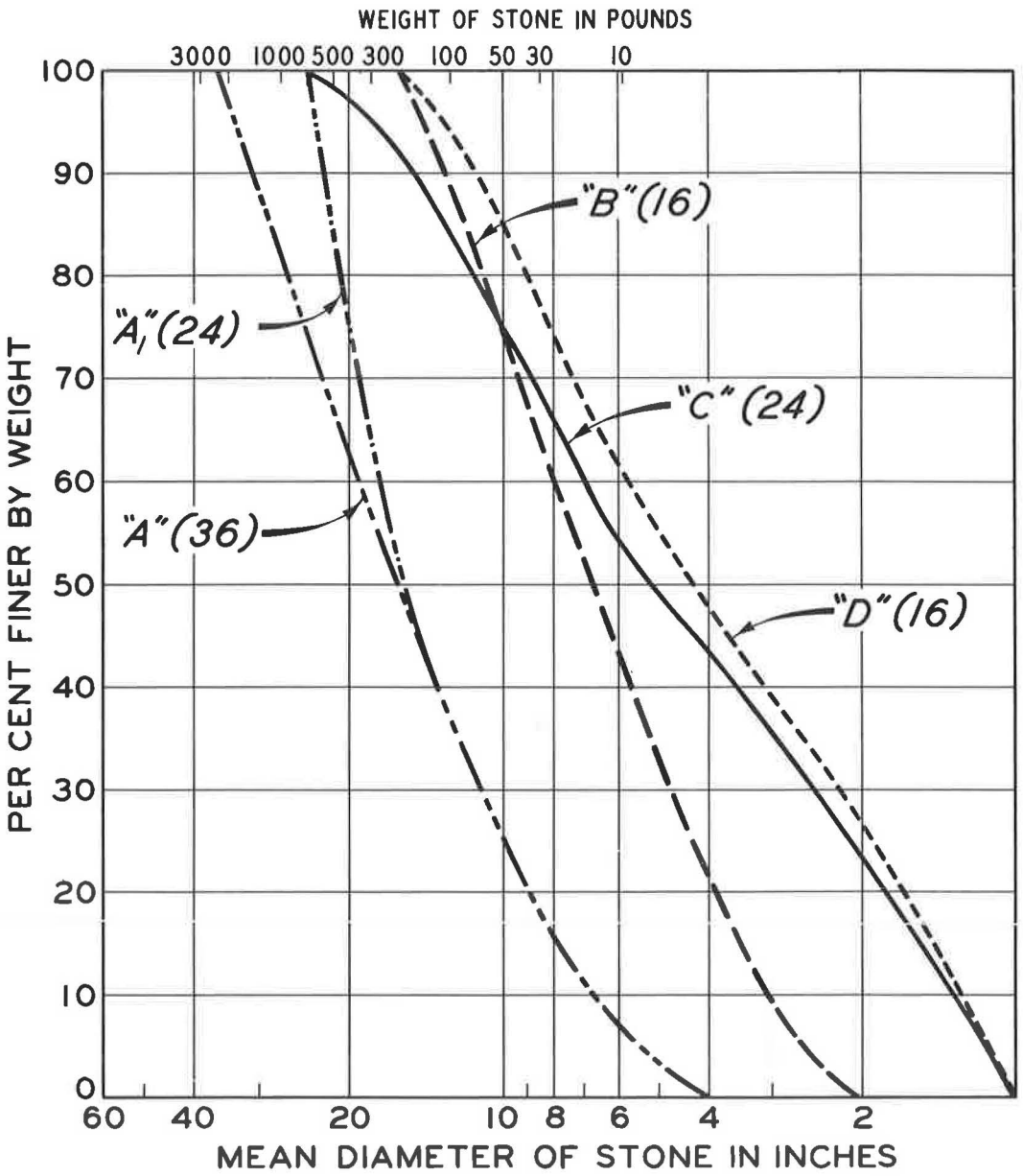


Figure 3. Protective stone gradation curves.

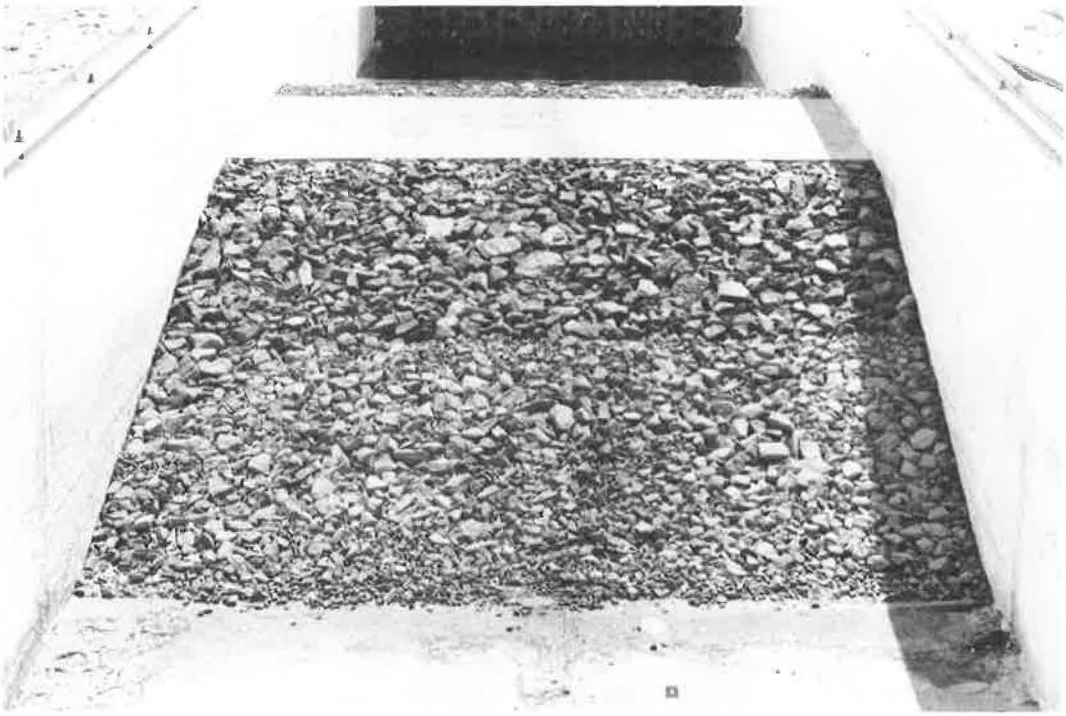

Figure 4. Test section prior to test.

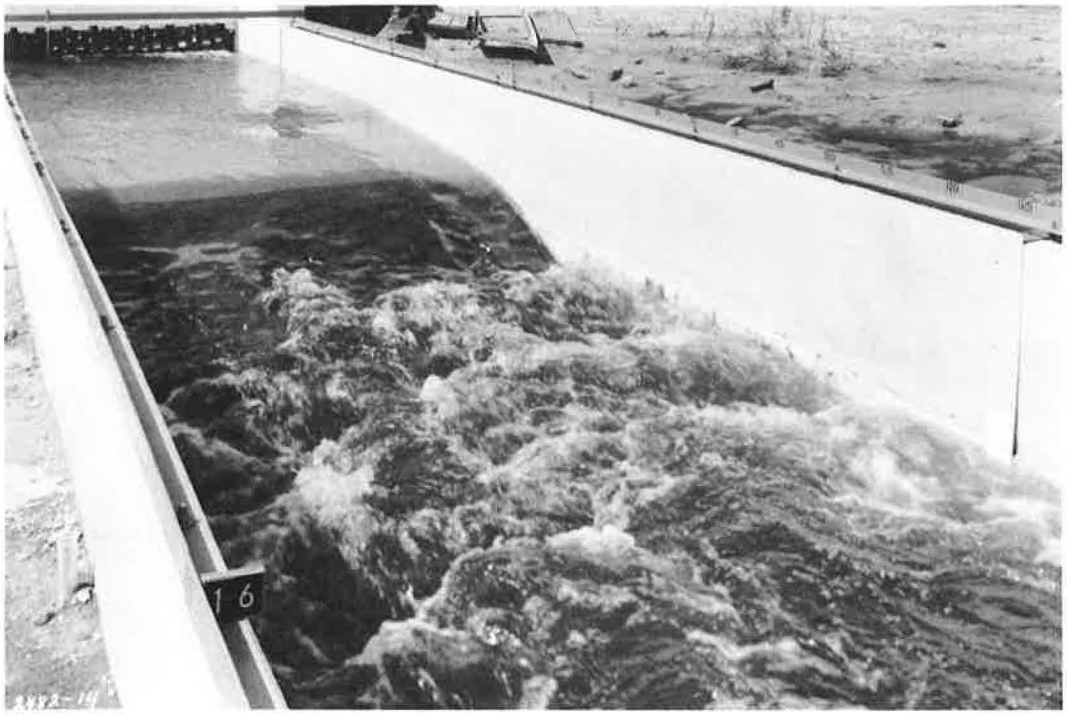


Figure 5. Flow through model, 20 cfs.


Figure 6. Flow through model, 60 cfs.

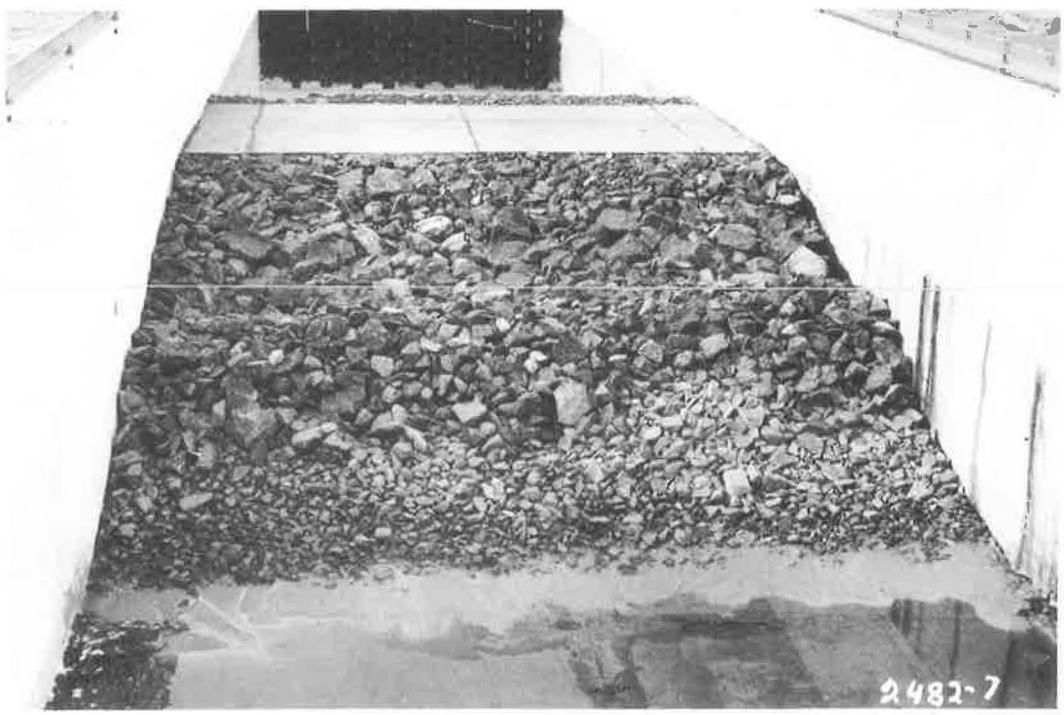


Figure 7. Disturbed test section.

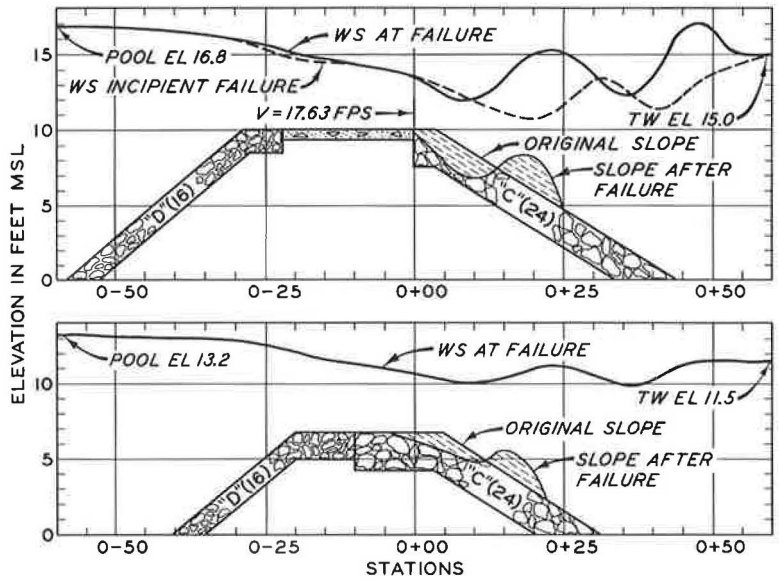


WATER-SURFACE AND SCOUR PROFILES

Figure 8. Typical profile plots.

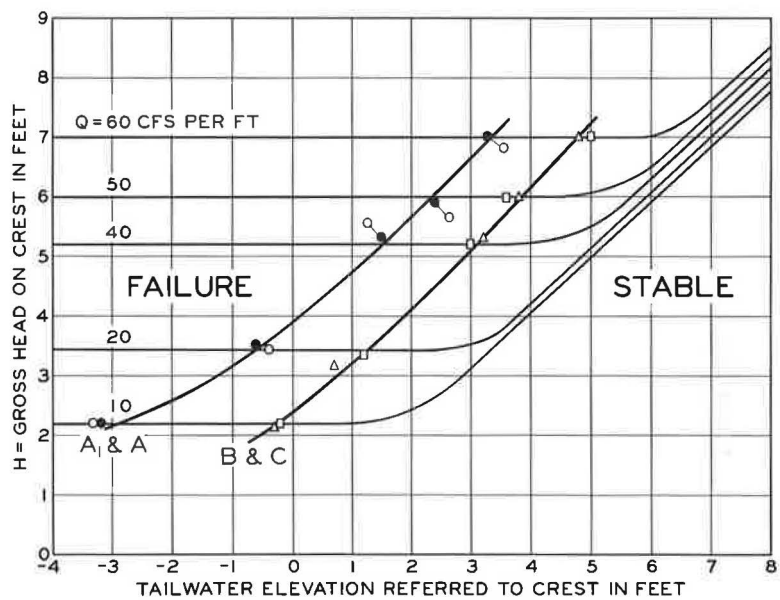


ACCESS TYPE EMBANKMENT

Figure 9. Headwater-tailwater for failure of access embankment.

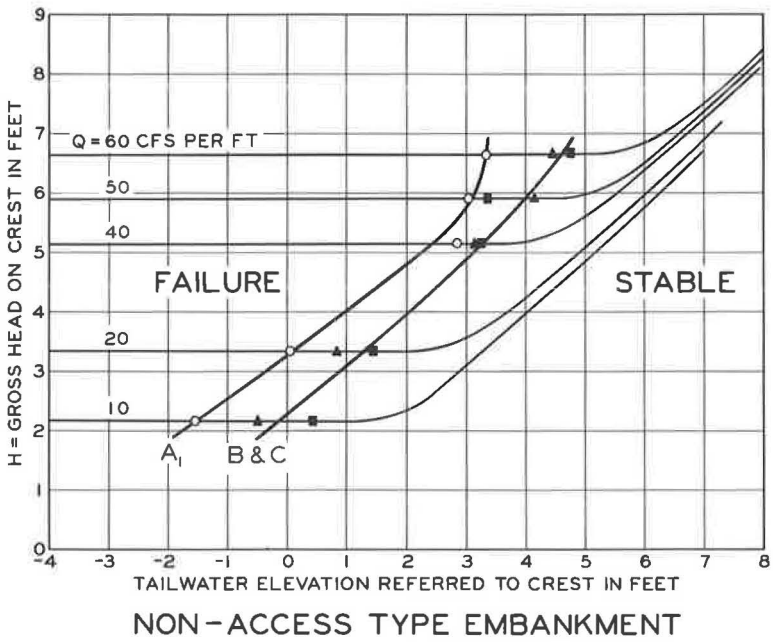


Figure 10. Headwater-tailwater for failure of non-access embankment.

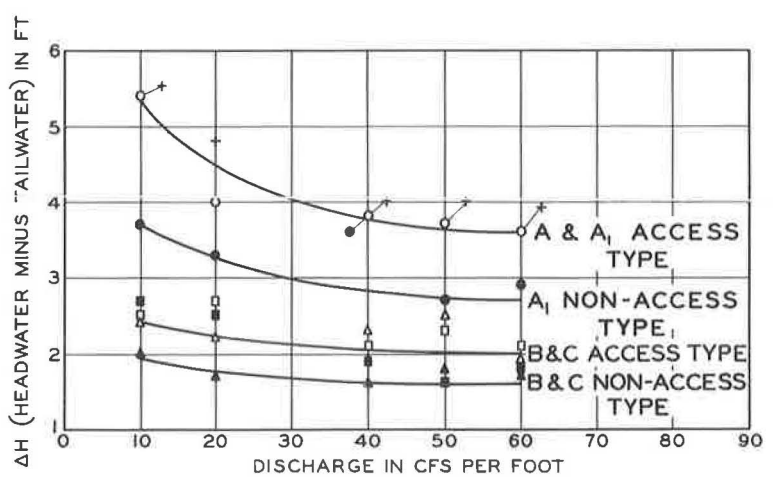


Figure 11. Conditions of failure.

Figure 11 plots the head differentials at which failure occurred. At the high discharges, 40, 50, and 60 cfs per ft, this differential was found to be essentially constant for a particular set of embankment conditions. However, failure of a particular gradation of riprap occurred at a lower differential on the non-access type embankment than it did on the access type. The reason for this must be due either to the difference in crown widths, 32.5 ft for access type and 24.5 ft for non-access type, or to flow percolating from the headwater through the upper layers of rock in the non-access type embankment and exerting added uplift pressures on the rock in the failure zone.

Various means of plotting the data in a dimensionless form in order to make its application more general have been attempted without success. However, fortunately, or maybe unfortunately for the profession in general, the prime requirements of the designers of the Arkansas River overflow embankments have been satisfied.